

## Accepted Manuscript

Title: Dimensionality imprint of electrical anisotropy in magnetotelluric responses

Authors: A. Martí, P. Queralt, J. Ledo, C. Farquharson

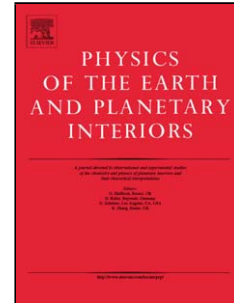
PII: S0031-9201(10)00149-4  
DOI: doi:10.1016/j.pepi.2010.07.007  
Reference: PEPI 5314

To appear in: *Physics of the Earth and Planetary Interiors*

Received date: 6-4-2010  
Revised date: 8-7-2010  
Accepted date: 15-7-2010

Please cite this article as: Martí, A., Queralt, P., Ledo, J., Farquharson, C., Dimensionality imprint of electrical anisotropy in magnetotelluric responses, *Physics of the Earth and Planetary Interiors* (2010), doi:10.1016/j.pepi.2010.07.007

This is a PDF file of an unedited manuscript that has been accepted for publication. As a service to our customers we are providing this early version of the manuscript. The manuscript will undergo copyediting, typesetting, and review of the resulting proof before it is published in its final form. Please note that during the production process errors may be discovered which could affect the content, and all legal disclaimers that apply to the journal pertain.



1

2

3

4

5

6

**Dimensionality imprint of electrical anisotropy in magnetotelluric  
responses**

7

8

9

**Martí, A.<sup>1</sup>, P. Queralt<sup>1</sup>, J. Ledo<sup>1</sup>, C. Farquharson<sup>2</sup>**

10

<sup>1</sup>: Departament de Geodinàmica i Geofísica. Universitat de Barcelona, Spain.

11

<sup>2</sup>: Earth Sciences Department. Memorial University of Newfoundland, Canada.

12

[annamarti@ub.edu](mailto:annamarti@ub.edu)

13

14

Submitted to Physics of the Earth and Planetary Interiors

15

16

Version 2. July 2010

17

18 **Abstract**

19 Dimensionality analysis of magnetotelluric data is a common procedure for inferring the  
20 main properties of the geoelectric structures of the subsurface such as the strike  
21 direction or the presence of superficial distorting bodies, and enables the most  
22 appropriate modeling approach (1D, 2D or 3D) to be determined. Most of the methods  
23 currently used assume that the electrical conductivity of individual parts of a structure is  
24 isotropic, although some traces of anisotropy in data responses can be recognized. In  
25 this paper we investigate the imprints of anisotropic media responses in dimensionality  
26 analysis using rotational invariants of the magnetotelluric tensor. We show results for  
27 responses generated from 2D synthetic anisotropic models and for field data that have  
28 been interpreted as showing the effects of electrical anisotropy in parts of the subsurface  
29 structure. As a result of this study we extend the WAL dimensionality criteria to include  
30 extra conditions that allow anisotropic media to be distinguished from 2D isotropic  
31 ones. The new conditions require the analysis of the strike directions obtained and take  
32 into account the overall behavior of different sites in a survey.

33

## 34 **1. Introduction**

35 Electrical anisotropy in the Earth, caused by electrical conductivity varying with  
36 orientation, is a property that is increasingly being taken into account in the  
37 interpretation of magnetotelluric data. Electrical anisotropy in the crust can be caused  
38 by preferred orientations of fluids, sulfides or fractures (Wannamaker, 2005), whereas  
39 in the upper mantle, it is linked to the splitting of seismic SKS waves (Eaton and Jones,  
40 2006), and is explained by either hydrogen diffusivity in olivine crystals (Wannamaker,  
41 2005; Wang et al., 2006) or by the presence of partial melt elongated in the direction of  
42 plate motion (Yoshino et al, 2006).

43

44 Significant developments have been achieved regarding the study of electrical  
45 anisotropy using magnetotellurics. These deal with modelling and inversion schemes,  
46 which include anisotropy (Pek and Verner, 1997; Weidelt, 1999; Wang and Fang, 2001;  
47 Li, 2002; Yin, 2003; Pek and Santos, 2002, 2006), the analysis of magnetotelluric  
48 responses affected by anisotropy (Reddy and Rankin, 1975; Saraf et al., 1986; Osella  
49 and Martinelli, 1993; Heise and Pous, 2003; Heise et al., 2006), and the investigation of  
50 the intrinsic properties and processes causing electric anisotropy (Gatzemeier and  
51 Tommasi, 2006). Some of the aforementioned papers were published in a special issue  
52 dedicated to electrical and seismic continental anisotropy (Eaton and Jones, 2006). A  
53 review of earlier work can be found in Wannamaker (2005).

54

55 To date there have been no studies specifically discussing the effects of anisotropy on  
56 rotational invariants or its complete dimensionality characterization. The goal of this  
57 paper is to identify electrical anisotropy using dimensionality analysis based on the  
58 rotational invariants of the magnetotelluric tensor. Data were generated from various

59 synthetic models with electrical anisotropy using the 2D code of Pek and Verner (1997).  
60 The results from a set of field data that has been interpreted as exhibiting the effects of  
61 anisotropic Earth structure (from the COPROD dataset) are also discussed.

62

63

## 64 **2. Background**

### 65 **2.1. Dimensionality analysis in magnetotellurics**

66 In the magnetotelluric (MT) method (e.g. Vozoff, 1991; Simpson and Bahr, 2005),  
67 dimensionality analysis is a common procedure for determining, prior to modeling,  
68 whether the measured data or computed responses (impedance tensor,  $\underline{Z}$ ; tipper,  $\mathbf{T}$ ;  
69 apparent resistivities,  $\rho_{ij}$ ; and phases,  $\varphi_{ij}$ ) at a given frequency ( $\omega$ ) correspond to 1D, 2D  
70 or 3D geoelectrical structures. It also allows identification and quantification of  
71 distortions (Kaufman, 1988; Groom and Bailey, 1989; Smith, 1995) and, when  
72 applicable, recovery of the directionality (strike) of the structures. Dimensionality  
73 analysis techniques search for particular relationships between the components of the  
74 magnetotelluric impedance tensor,  $\underline{Z}(\omega)$  (e.g. Cantwell, 1960), or related functions, in  
75 order to identify each dimensionality type. Additional information can be obtained from  
76 the induction arrows (i.e., tipper vectors). The dimensionality analysis technique that  
77 sees the most widespread use is that of McNeice and Jones (2001). This technique uses  
78 the Groom and Bailey (1989) decomposition method to find the best fitting 2D  
79 parameters for a set of sites at different period bands. Lilley (1993) introduced the use  
80 of Mohr circles to display and analyze magnetotelluric data, allowing to distinguish  
81 their dimensionality and the presence of galvanic distortion. In two-dimensional cases,  
82 the regional geologic strike is estimated from either the real or imaginary parts of the  
83 magnetotelluric tensor ( $\theta_{hr}$ ,  $\theta_{hq}$ , eqs. 113 and 114, Lilley, 1998a). Lilley and Weaver

84 (2009) presented a Mohr circles analysis for data with phases out of quadrant, although  
85 not particularly related with anisotropy.

86

87 Weaver et al. (2000) (based on Lilley, 1993, 1998a; Fisher and Masero, 1994; and  
88 Szarka and Menvielle, 1997) presented a complete dimensionality criteria based on the  
89 rotational invariants (WAL invariants) of the magnetotelluric tensor ( $\underline{M}(\omega)$ ), defined as  
90 the relationship between the electric field  $\underline{E}(\omega)$  and the magnetic induction  $\underline{B}(\omega)$ ;  
91  $\underline{M}(\omega) = (1/\mu_0)\underline{Z}(\omega)$ . The WAL rotational invariants comprise seven independent ( $I_1$ ,  
92  $I_2$ ,  $I_3$ ,  $I_4$ ,  $I_5$ ,  $I_6$  and  $I_7$ ) parameters and one dependent (Q) parameter. They can be  
93 represented by Mohr circle diagrams (Lilley, 1993) (Figure 1), and, except  $I_1$  and  $I_2$ ,  
94 they are taken as sines of angles, which implies an ambiguity in the quadrant to which  
95 each angle belongs. Also with the exception of  $I_1$  and  $I_2$ , they are dimensionless and  
96 normalized to unity, with their vanishing having a physical interpretation that is related  
97 to the geoelectric dimensionality (see Weaver et al., 2000, for a full description of the  
98 invariants).

99

100 WAL dimensionality criteria, based on the vanishing or not of some of the invariants ( $I_3$   
101 to  $I_7$ ), are summarized in Table 1. Dimensionality analysis using WAL criteria has been  
102 implemented, including data errors and band averages (Martí et al., 2004), in the  
103 WALDIM code (Martí et al., 2009). Given that on field, therefore noisy data, the  
104 invariants are rarely precisely zero, the program uses two threshold values (as suggested  
105 by Weaver et al., 2000):  $\tau$ , for  $I_3$  to  $I_7$ ; and  $\tau_Q$ , for invariant Q; below which the  
106 invariants are taken to be zero.

107

108 It is also important to note the parameters that can be derived from the invariants for  
 109 specific dimensionality cases: In 1D cases, invariants  $I_1$  and  $I_2$  provide information  
 110 about the 1D magnitude and phase of the geoelectric resistivity ( $\rho_{1D}$  and  $\varphi_{1D}$ ). In 2D,  
 111 the strike angle (referred to as  $\theta_{2D}$ ) can be obtained from the real and imaginary parts of  
 112 the MT tensor, with  $\theta_1$  and  $\theta_2$  giving the same value for the strike angle (see expressions  
 113 in the Appendix). In 2D cases affected by galvanic distortion (identified as 3D/2D), the  
 114 strike angle ( $\theta_{3D/2D}$ ) is computed considering both the real and imaginary parts of the  
 115 MT tensor and the distortion parameters, as  $\phi_1$  and  $\phi_2$  (Smith, 1995), which are linear  
 116 combinations of the Groom and Bailey (1989) twist and shear angles ( $\varphi_t = \phi_1 + \phi_2$ , and  
 117  $\varphi_e = \phi_1 - \phi_2$ ). In 2D cases (which are particular cases of 3D/2D), the strikes computed as  
 118  $\theta_1$ ,  $\theta_2$  and  $\theta_{3D/2D}$  (see Appendix) are equivalent and the values of  $\varphi_t$  and  $\varphi_e$  are  
 119 negligible.

120

121 It must be remembered that the WAL criteria, as well as the other dimensionality  
 122 analysis methods, are based on the assumption that the geoelectrical structures are  
 123 isotropic.

124

125 Another tool used to infer the dimensionality in isotropic media is the phase tensor  
 126 (Caldwell et al., 2004), which is not affected by galvanic distortion (hence only 1D, 2D  
 127 and 3D cases can be identified). It can be represented by an ellipse, characterized by 4  
 128 parameters, the 3 rotational invariants  $\Phi_{Max}$ ,  $\Phi_{min}$  (principal directions) and  $\beta$ , and the  
 129 non invariant angle  $\alpha$  (see Caldwell, 2004, for a more detailed description). In 1D cases,  
 130 the ellipses are circles ( $\Phi_{Max} = \Phi_{min}$ ). In 2D,  $\Phi_{Max}$  and  $\Phi_{min}$  have different values,  $\alpha$   
 131 indicates the strike direction and  $\beta$  is null. In 3D,  $\beta$  is non-zero. Heise et al. (2006) used

132 the phase tensor diagrams to represent the responses of models with electric anisotropy.  
 133 We will compare the phase tensor analysis with the WAL dimensionality criteria for  
 134 some of the examples presented below.

135

## 136 2.2. Electrical anisotropy and modelling

137 The properties of an anisotropic medium need to be expressed in a tensor form. For the  
 138 case of electrical anisotropy, the conductivity ( $\sigma$ , reciprocal of the resistivity  $\rho$ ,  $\sigma = 1/\rho$ )  
 139 adopts the general form of a symmetric tensor with non-negative components,

140

$$141 \quad \sigma = \begin{bmatrix} \sigma_{xx} & \sigma_{xy} & \sigma_{xz} \\ \sigma_{yx} & \sigma_{yy} & \sigma_{yz} \\ \sigma_{zx} & \sigma_{zy} & \sigma_{zz} \end{bmatrix}, \quad (1)$$

142

143 where x (North), y (East) and z (vertically downwards) are the orthogonal axes of a  
 144 Cartesian coordinate system. The conductivity tensor can represent an intrinsic property  
 145 of the material (microscopic anisotropy) (Negi and Saraf, 1989), or it can represent the  
 146 result of mixing in a preferred orientation of two or more media with differing  
 147 conductivities (macroanisotropy) (e.g. Wannamaker, 2005). The resolving power of the  
 148 MT method and the depths at which anisotropic media are typically located (lower  
 149 crust, upper mantle), usually make it impossible to distinguish between them (Weidelt,  
 150 1999).

151

152 Using Euler's elementary rotations the conductivity tensor can be diagonalised and its  
 153 principal directions obtained, namely the strike, dip and slant anisotropy angles ( $\alpha_s$   
 154 around z-axis,  $\alpha_D$  around x'-axis and  $\alpha_L$  around z''-axis) (Figure 2). Hence, the



155 conductivity tensor can be specified by six parameters: the three conductivity  
156 components along the principal directions ( $\sigma'_{xx}$ ,  $\sigma'_{yy}$  and  $\sigma'_{zz}$ ) and their  
157 corresponding angles.

158

159 Particular cases of anisotropy, specified in terms of the relationships between the  
160 components along the principal directions of the conductivity tensor, are azimuthal  
161 anisotropy ( $\sigma'_{xx} = \sigma'_{zz}$  or  $\sigma'_{yy} = \sigma'_{zz}$ , anisotropy in only one direction, x or y) and  
162 uniaxial anisotropy ( $\sigma'_{xx} = \sigma'_{yy} \neq \sigma'_{zz}$ ). In the latter, anisotropy can only be identified  
163 by the vertical component of the electric and magnetic fields (Negi and Saraf, 1989).

164

165 For anisotropic media, the MT forward problem must be solved, in general, using a  
166 numerical approach. The code of Pek and Verner (1997) uses the finite-difference  
167 method to obtain the responses for 1D and 2D anisotropic media.

168

169 The magnetotelluric responses obtained from an anisotropic medium are characterized  
170 by resistivity shifts, phase splits (which are related to anisotropy contrasts rather than  
171 bulk anisotropy of the medium Heise et al., 2006), and induction arrows not correlated  
172 to the principal direction indicated by the MT tensor (Pek and Verner, 1997; Weidelt,  
173 1999).

174

175

### 176 **3. Dimensionality analysis of synthetic anisotropic model responses using** 177 **WALDIM**

178 In this section we present some examples for synthetic models with anisotropy, the  
179 responses of which have been calculated using the code of Pek and Verner (1997). In

180 these, we have performed the dimensionality analysis using the WALDIM code and we  
181 have analyzed the results indicating which features are characteristic of the anisotropic  
182 structures.

183

184 The models were chosen to increase gradually in complexity starting from the most  
185 simple. Only 2D situations, not 3D situations, are considered in this study as it is not  
186 possible to separate the imprint of anisotropy from 3D effects.

187

188 Except when indicated, all the models have dimensions of 860 km (y, towards East) by  
189 186 km (z, vertical downwards), and are discretised using 40 (y) by 30 (z) cells, plus 11  
190 air layers. The responses were computed at each surface node, at the periods indicated  
191 in the sections below, following the  $e^{+i\omega t}$  convention for the time-harmonic factor of the  
192 electric and magnetic fields. WALDIM analysis was performed for each resulting MT  
193 tensor, with 1% random noise having been added to each component. Threshold values  
194 of  $\tau = 0.1$  and  $\tau_Q = 0.1$ , which were tested to be consistent with the noise level applied,  
195 were used. We also tested, by representing the results using Mohr circle diagrams  
196 (following Lilley, 1998b), that the invariant values are obtained as sines of positive  
197 angles within the range  $0^\circ - 90^\circ$ ; and that the dimensionality description obtained from  
198 the invariant parameters and Mohr circles are consistent.

199

### 200 3.1 ANISOTROPIC HALF-SPACE

201 For the simplest cases, we considered three models consisting of anisotropic half-  
202 spaces.

203

204 The three models have azimuthal anisotropy with the same resistivity values,  $\rho'_{xx} = 50$   
 205  $\Omega\cdot\text{m}$  and  $\rho'_{yy} = \rho'_{zz} = 500 \Omega\cdot\text{m}$ , and are distinguished from each other by the orientation  
 206 of the principal directions. In the first model (**1a**), these coincide with the measurement  
 207 axes. In the second (**1b**), these have been rotated through a strike angle  $\alpha_s = 40^\circ$  around  
 208 the z axis. In the third model (**1c**), a general rotation using dip ( $55^\circ$ ) and slant ( $20^\circ$ )  
 209 angles has been considered (see Table 2). The responses for each model were computed  
 210 at  $T = 1 \text{ s}, 3.2 \text{ s}, 10 \text{ s}, 32 \text{ s}, 100 \text{ s}$  and  $320 \text{ s}$ .

211

212 For the three models, the responses are site independent, and only show slight variations  
 213 with period due to numerical inaccuracies. Apparent resistivity values depend on the  
 214 projection of the anisotropy direction on to the x and y axes, as shown in Figure 3a.  
 215 Phase values (not shown in the figure) of the off-diagonal components are  $45^\circ$  (xy  
 216 polarization) and  $-135^\circ$  (yx polarization) (as expected from a medium without vertical  
 217 variations in resistivity). For model **1a**, xx and yy apparent resistivities are zero, and  
 218 hence, the corresponding phases are undetermined. In contrast, for models **1b** and **1c**, xx  
 219 and yy phases are  $45^\circ$  and  $-135^\circ$  respectively. These responses, observed at a particular  
 220 site, could be interpreted as a case of galvanic distortion (with shear and anisotropy  
 221 effects) over a homogeneous medium.

222

223 Regarding the dimensionality analysis results, invariant values present similar  
 224 relationships for the three models, for all sites and frequencies:  $I_3 = I_4 > \tau$ ,  $I_5$  and  $I_6 < \tau$   
 225 and  $Q < \tau_Q$ . The exception is  $I_7$ , with values either below or above the threshold value,  
 226 due to random noise effects. The WAL criteria define the dimensionality as 2D for all  
 227 models (Figure 3a) and the strike directions are well defined:  $\theta_1 \approx \theta_2 (= \theta_{2D})$ , with small  
 228 errors, also due to the noise added. For models **1a** and **1b**, these angles are coincident

229 with  $\alpha_S$  ( $0^\circ$  deg or  $40^\circ$  respectively), and for model **1c** it is  $12^\circ$ , due to the projection onto  
 230 the horizontal plane of the new  $x'$  and  $y'$  axes, resulting from the dip and slant rotations.  
 231 The dimensionality and the strike direction also agree with the Mohr diagrams ( $\theta_{hr} \approx \theta_{hq}$   
 232  $\approx \theta_1 \approx \theta_2 = 12^\circ$ ), as shown for model **1c** in Figure 3b.

233

234 For models **1b** and **1c**, for which the anisotropy directions are not aligned with the  
 235 measuring axes, two particular features are observed:  $\theta_{3D/2D}$  values (which cannot be  
 236 represented using Mohr circles) are unstable and are different from  $\theta_{2D}$  (Figure 3a). This  
 237 does not happen in isotropic 2D structures. In the appendix, the analytical expressions  
 238 used to obtain the strike directions for the magnetotelluric tensors corresponding to a 2D  
 239 isotropic model and an anisotropic half-space are developed. In the anisotropic case, the  
 240 value of  $\theta_{3D/2D}$  is indeterminate, but in the responses of the synthetic model its values  
 241 are unstable due to the effects of the noise. The main result is that both the analytic  
 242 expressions and the responses prove that  $\theta_{2D}$  and  $\theta_{3D/2D}$  are not coincident in the case of  
 243 an anisotropic half-space.

244

245 For the three models, phase tensors (Caldwell et al., 2004; Heise et al., 2006) would be  
 246 represented by unit circles independent of the orientation of the principal directions, and  
 247 would thus provide no hint of anisotropy.

248

249 In model **1a**, the fact that all site responses are the same whilst the dimensionality is 2D  
 250 indicate that either all the measuring sites are aligned with the strike direction or that the  
 251 structure is not isotropic but anisotropic. Hence, when the anisotropic directions are  
 252 coincident with the measuring axes, the responses do not allow the presence of  
 253 anisotropy in a half-space to be distinguished. In contrast, when anisotropy is not

254 aligned with the measuring axes (models **1b** and **1c**), the non agreement between the  
 255 values of the strike directions  $\theta_{2D}$  and  $\theta_{3D/2D}$  is an indication that the half-space over  
 256 which the measurements are obtained is indistinctly anisotropic. This is an important  
 257 result, given that it is common to state that 1D anisotropic media are indistinguishable  
 258 from 2D isotropic media. This type of anisotropic structure cannot be identified using  
 259 the phase tensor.

260

### 261 3.2 1D MEDIA WITH ONE AND TWO ANISOTROPIC LAYERS

262 The first one-dimensional model presented here (model **2a**) was taken from one of the  
 263 examples provided with the Pek and Verner (1997) code. It consists of a layered  
 264 structure with an embedded anisotropic layer (Figure 4): ( $\rho'_{xx} = 1 \text{ } \Omega \cdot \text{m}$  and  
 265  $\rho'_{yy} = \rho'_{zz} = 100 \text{ } \Omega \cdot \text{m}$ , and  $\alpha_S = 30^\circ, \alpha_D = 0^\circ, \alpha_L = 0^\circ$ ). The model responses were  
 266 computed at 10 periods between  $T = 1 \text{ s}$  to  $T = 32000 \text{ s}$ .

267

268 The MT responses, which are shown in Figure 4, are the same at all sites.. Diagonal  
 269 responses are coincident ( $xx = yy$ ), whereas the off-diagonal responses show a split  
 270 between the polarizations. The off-diagonal resistivity and phases are plotted together  
 271 with the responses ( $xy = yx$ ) of two models in which the anisotropic layer is replaced  
 272 with an isotropic one; the first model with a  $1 \text{ } \Omega \cdot \text{m}$  layer, and the second with a  $100$   
 273  $\Omega \cdot \text{m}$  layer (Figure 4). Because of the rotation ( $\alpha_S$ ) of the principal directions, the values  
 274 of the off-diagonal resistivities and phases for the model with the anisotropic layer are  
 275 smoother than those for the models with the isotropic layers.

276

277 The WAL dimensionality criteria ( $I_3 = I_4 > \tau$ ,  $I_5, I_6$  and  $I_7 < \tau$  and  $Q > \tau_Q$ ) indicate 2D  
 278 structures with  $\theta_{2D} = 30^\circ (= \alpha_S)$  for all periods (Figure 4), except for  $T=1 \text{ s}$  at which the

279 criteria indicate 1D structure because the skin depth (5 km) is smaller than the top of the  
 280 anisotropic layer. For the periods at which 2D structure is indicated, the strike direction  
 281 computed as  $\theta_{3D/2D}$  is coincident with  $\theta_{2D}$  and the distortion parameters are practically  
 282 null.

283

284 The effects of the inclusion of a second anisotropic layer just below the first one were  
 285 also investigated by considering the third layer of model **2a** to be anisotropic as well. In  
 286 the first of these models (model **2b**), this new anisotropic layer has the same resistivity  
 287 values as the upper one, but with the main directions rotated at an angle  $\alpha_S = 45^\circ$ . In the  
 288 second model (model **2c**), both the resistivity values ( $\rho'_{xx} = 1 \Omega \cdot m$  and  $\rho'_{yy} = \rho'_{zz} = 10$   
 289  $\Omega \cdot m$ ) and  $\alpha_S$  ( $45^\circ$ ) were changed in the new layer. The dimensionality pattern for both  
 290 (Figure 5) is, from the shortest to the longest period: 1D (corresponding to the first  
 291 isotropic layer), 2D with a  $30^\circ$  strike direction (corresponding to the first anisotropic  
 292 layer), 3D (due to an abrupt increase in the value of invariant  $I_7$  caused by the inclusion  
 293 of the second anisotropic layer), and finally 2D, with an approximately  $39^\circ$  strike, a  
 294 value in between the two anisotropy strike values of the two layers ( $30^\circ$  and  $45^\circ$ ). In all  
 295 the 2D cases, as had happened in the case with a single anisotropic layer, the directions  
 296  $\theta_{2D}$  and  $\theta_{3D/2D}$  are coincident.

297

298 We can summarize that in a 1D medium with one anisotropic layer, dimensionality is  
 299 2D with a well defined angle  $\theta_{2D}$  (equivalent to  $\alpha_S$ , or a projection of the anisotropic  
 300 directions onto the horizontal if other rotations have been performed), which has the  
 301 same value as  $\theta_{3D/2D}$ , as would happen in an isotropic medium. In this case the only hint  
 302 that anisotropy is present is the fact that the responses are the same at all sites, except  
 303 when the anisotropy angle is  $0^\circ$ , for which responses are equivalent to those of a 2D

304 model with measurements along the strike direction. When two different anisotropic  
 305 layers are considered, the dimensionality varies with period: from 2D (corresponding to  
 306 the first anisotropic layer), to 3D, and back to 2D.

307

### 308 3.3 2D ANISOTROPIC MEDIA

309 In this section, we considered two groups of models based on the examples used in  
 310 Reddy and Rankin (1975) and Heise et al. (2006). The first group contains models in  
 311 which the electrical properties vary only in the horizontal direction; the models in the  
 312 second group possess more general two-dimensional variations.

313

314 - Anisotropic dyke:

315 The models in the first group (Figure 6) consist of a vertical dyke intruded into a  
 316 medium with differing electrical properties. Initially we consider a model in which both  
 317 the dyke and the surroundings are isotropic (model **3a**,  $\rho_{dyke} = 10 \text{ } \Omega \cdot \text{m}$  and  
 318  $\rho_{surroundings} = 100 \text{ } \Omega \cdot \text{m}$ ). A second model (model **3b**) consists of an anisotropic dyke  
 319 ( $\rho'_{xx} = 3 \text{ } \Omega \cdot \text{m}$ ,  $\rho'_{yy} = 10 \text{ } \Omega \cdot \text{m}$ ,  $\rho'_{zz} = 20 \text{ } \Omega \cdot \text{m}$ , and  $\alpha_S = 30^\circ, \alpha_D = 0^\circ, \alpha_L = 0^\circ$ )  
 320 sandwiched by an isotropic medium of  $\rho = 100 \text{ } \Omega \cdot \text{m}$ . In the third model, both the dyke  
 321 and the surroundings are anisotropic. The responses for the three models were computed  
 322 at one period per decade between  $T = 1 \text{ s}$  and  $T = 10000 \text{ s}$ .

323

324 For the isotropic model, **3a**, the dimensionality is 1D at sites located outside and far  
 325 from the dyke (Figure 6a). Inside and surrounding the dyke, the dimensionality is 2D ( $0^\circ$   
 326 strike), except at the first periods for the sites located at the centre of the dyke for which  
 327 the dimensionality is 1D. At these periods these sites are too far from, and hence not  
 328 affected by, the dyke boundaries.

329

330 For model **3b** (anisotropic dyke surrounded by an isotropic medium), the dimensionality  
331 pattern outside the dyke is similar to that of model **3a** (Figure 6b): mainly 1D and 2D  
332 (with  $0^\circ$  strike). At the edges of the dyke and at the longest periods the dimensionality is  
333 3D/1D2D. For sites located over the dyke is the dimensionality is 3D, except for the  
334 shortest periods at the central part, for which with the dimensionality is 2D with a strike  
335 of  $30^\circ$ . In these 2D cases, the strike direction is coincident with the anisotropy angle  $\alpha_S$ .  
336 However, the direction given by  $\theta_{3D/2D}$  has a different value ( $60^\circ$ ) from that of  $\theta_{2D}$  ( $30^\circ$ ),  
337 in contrast to what was observed for the anisotropic half-space models (models **1b** and  
338 **1c**), and the distortion parameters are not negligible ( $\varphi_t = 2^\circ$  and  $\varphi_e = -14^\circ$ ).

339

340 When both the dyke and surroundings are anisotropic (model **3c**), the dimensionality is  
341 more complex. Nevertheless there are clear differences with to the results observed for  
342 the previous models **3a** and **3b**, and there are distinctive features associated with each  
343 region of the model (Figure 6c). Outside the dyke and far from its edges the  
344 dimensionality is 2D with  $\theta_{2D} = 55^\circ$ , which is different from the value given by  $\theta_{3D/2D}$   
345 (with variable values, as shown in Figure 6c). Still outside but closer to the dyke edges,  
346 the dimensionality is mainly 3D/2D with a strike direction of around  $75^\circ$  or  $80^\circ$  and  
347 distortion parameters  $\varphi_t$  negligible and  $\varphi_e = -10^\circ$ . At the edges, is the dimensionality is  
348 either 3D/2D or 3D/1D2D. The 3D/2D cases obtained both outside the dyke and at the  
349 edges have the peculiarity that, according to the invariant parameters, the  
350 dimensionality should be 2D, but the strike directions are inconsistent ( $\theta_1 \neq \theta_2$ ). It  
351 would therefore not be possible to rotate and obtain a regional 2D tensor. Instead, the  
352 impedance tensor is better described as 3D/2D with the  $\theta_{3D/2D}$  strike and distortion  
353 angles that are small but not negligible (Martí et al., 2009). The use of these strike and



354 distortion angles allows, in isotropic structures, the decomposition of the impedance  
 355 tensor to be performed and a 2D tensor recovered. Inside the dyke, at the shortest  
 356 period, the dimensionality is 2D, with  $\theta_{2D} = 30^\circ = \alpha_S$ , inconsistent with  $\theta_{3D/2D}$  ( $70^\circ$ ), and  
 357 with non-negligible values of the shear distortion angle ( $\varphi_e = -10^\circ$ ). As the period  
 358 increases, the dimensionality becomes 3D, 3D/2D (with  $\theta_{3D/2D} = 75^\circ$ ,  $\varphi_t = -12^\circ$  and  $\varphi_e =$   
 359  $-10^\circ$ ), and finally 3D/1D2D.

360

361 From the above dimensionality description, the presence of anisotropy can be  
 362 recognized in the 2D cases, for which the strike directions given by  $\theta_{2D}$  (which agree  
 363 with the anisotropic azimuth) and  $\theta_{3D/2D}$  are different (Figure 6). Moreover, there are  
 364 also cases that should be 2D according to the invariants, but for which  $\theta_1 \neq \theta_2$ .  
 365 Therefore, these cases are described as 3D/2D, with the strike direction ( $\theta_{3D/2D}$ ,  
 366 computed from the real and imaginary parts of the tensor) close to the sum of both  
 367 anisotropic directions ( $80^\circ$ ).  $\theta_{hr}$  and  $\theta_{hq}$  do not provide the correct strike direction either,  
 368 as they are computed using the real or the imaginary parts separately. Also, for sites  
 369 over the dyke and at the edges, some 3D/1D2D and 3D cases are obtained.

370

371 - 2D conductive bodies and an anisotropic layer:

372 The second set of models is taken from the 2D examples used in Heise et al. (2006).  
 373 This set explores phase splits in responses from anisotropic structures, and the  
 374 identification of anisotropy using phase information (in particular, the phase tensor).

375

376 Model **4a** contains an anisotropic layer (with main directions along the x, y and z axes)  
 377 and two conductive blocks. Model **4b** is isotropic and contains two conductive blocks  
 378 similar to those in model **4a** (Figure 7). Heise et al. (2006) show how both models give

379 similar phase tensor and induction arrow responses, except at the longest periods, where  
380 the induction arrows for the isotropic model are significant, whereas in the anisotropic  
381 model they are almost null.

382

383 Rotational invariants and dimensionality of the responses of these two models were  
384 computed between 1 s and 30000 s (Figure 8). The invariants have similar values for  
385 both models, and hence the dimensionality displays similar patterns for both models. In  
386 general, the dimensionality is 1D for periods up to approximately 100 s, and 2D for the  
387 rest. However, the dimensionality of the first and last sites, located on top of the  
388 conductive blocks, is different for each model. For model **4a** dimensionality is 1D up to  
389 100 s, then becoming 2D as a consequence of the directionality introduced by the  
390 anisotropic layer, affecting all sites. For model **4b** all the cases are 1D as these sites are  
391 not affected by the lateral contrasts at the limits of the two conductive bodies. The phase  
392 tensor ellipses, which were computed for both models for the first site, also show this  
393 difference between the two models (Figure 9). These results confirm that for 2D models  
394 with anisotropic structures aligned with the main directions, both the invariants and the  
395 phase tensor provide the same information, and that for this example they cannot  
396 distinguish between the anisotropic and isotropic models.

397

398 Additionally, we considered model **4a** and modified the anisotropic layer by applying a  
399 rotation of the principal directions ( $\alpha_S = 30^\circ$ ). The dimensionality of the responses of the  
400 resulting model, identified as **4c**, is shown in Figure 8c. The dimensionality pattern is  
401 significantly more complex than for the previous models. Up to 100 s, the  
402 dimensionality is similar to that of models **4a** and **4b** (mostly 1D with 2D cases at the  
403 rightmost side of the model due to the shallow conductive structure). For periods around

404 100 s, most of the 1D cases become 2D ( $\theta_{2D}$  being consistent with  $\theta_{3D/2D}$ ) or 3D/2D  
405 (with an approximately 15° strike). At longer periods, the general trend is that the cases  
406 that were 1D and 2D in models **4a** and **4b** become 2D and 3D, respectively; with some  
407 3D/2D and 3D/1D2D exceptions. In all 3D/2D cases (most of them at 100 s), as  
408 happened for the model with the anisotropic dyke (**3c**), invariant values indicate 2D  
409 dimensionality, but, given that the two strike directions,  $\theta_1$  and  $\theta_2$ , are significantly  
410 different, the impedance tensor is better described as 3D/2D with  $\theta_{3D/2D}$ . This  
411 observation is a clear indication of the presence of anisotropy in the structures, with  
412 anisotropic directions non-aligned to the principal structural directions. In the phase  
413 tensor diagrams of these model responses (Figure 10) an equivalent effect can be  
414 observed at 100 seconds: the values of  $\beta$  are negligible (note that only angle values  
415 lower than 3° are considered negligible), whereas the main directions of the ellipse  
416 differ significantly from the strike angle  $\alpha$ .

417

418 Hence, for 2D models, both the WALDIM criteria and the phase tensor diagrams are  
419 able to identify the presence of anisotropic structures with principal directions not  
420 coincident with the measuring axes.

421

422

#### 423 **4. Anisotropy in field data: the COPROD dataset**

424 In this final section we refer to one case of field data that has been associated with  
425 anisotropy. This is the well known COPROD2 dataset, from southern Saskatchewan and  
426 Manitoba (Canada), which revealed the presence of the North American Central Plains  
427 conductivity anomaly (NACP) (Jones and Craven, 1990, Jones et al., 1993). This  
428 dataset was used to test inversion codes (see Jones, 1993). Some of the 2D models that

429 were obtained consisted of multiple isotropic high conductivity bodies separated by  
430 resistive regions. Jones (2006) revisited the data and, using one of the sites on top of the  
431 NACP anomaly as a reference (85\_314), proposed a 2D anisotropic model. This model  
432 consists of a thin superficial conductive layer ( $3 \Omega\cdot\text{m}$ ), a 100 km thick lithosphere of  
433  $1000 \Omega\cdot\text{m}$ , in which a single anisotropic block ( $\rho'_{xx} = 0.5 \Omega\cdot\text{m}$  along strike,  
434  $\rho'_{yy} = \rho'_{zz} = 1000 \Omega\cdot\text{m}$ ) is embedded, and a basal conducting layer of  $10 \Omega\cdot\text{m}$ . The off-  
435 diagonal responses for this model are in good agreement with those of the observed  
436 data, reproducing the split between TE and TM modes.

437

438 We computed the dimensionality for the synthetic tensors of the sites located over the  
439 anisotropic body. We obtained 1D cases, and 2D cases with  $0^\circ$  strike (anisotropy  
440 aligned with the measuring directions) (Figure 11a).

441

442 The data for site 85\_314 was used by Martí et al. (2009) as an example for  
443 dimensionality analysis using the WALDIM code. Up to 10 s, the data can be described  
444 as 1D. At periods longer than 10 s invariant values indicate 2D. However, at these  
445 periods strike angles  $\theta_1$  and  $\theta_2$  differ significantly, and hence the data were better  
446 described as 3D/2D, with a strike direction around  $80^\circ$  and small twist and shear  
447 distortion angles (lower than  $5^\circ$ ) (Figure 11b). This allowed 2D regional tensors to be  
448 obtained from tensor decomposition. According to the tests presented here, the  
449 discrepancy between the dimensionality descriptions from the model with the  
450 anisotropic block and the field data lies in the fact that in the synthetic data all the  
451 diagonal responses are null, whereas in the field data the values of the diagonal  
452 components, especially for the longest periods, are significant.

453

454 From our new characterization of anisotropy in dimensionality analysis, it is clear that  
455 the dimensionality of site 85\_314 is compatible with a 2D model that contains at least  
456 one anisotropic block or layer, having anisotropy directions aligned with the strike  
457 indicated in the dimensionality analysis (in this case of around  $80^\circ$ ). Hence, if the  
458 anisotropic block modeled by Jones (2006) had an anisotropic azimuth of  $80^\circ$ , the  
459 invariant values of the responses would correspond to 2D structures with two different  
460 strike directions  $\theta_1$  and  $\theta_2$ . This would be in agreement with the observed data.

461

462

#### 463 5. **WAL criteria extended to accommodate anisotropy**

464 The results obtained from this study have allowed specific relationships to be  
465 established between the invariants and strike directions that are linked to the presence of  
466 anisotropy. In general, these conditions are not recognized from a single tensor alone,  
467 but from the pattern at different sites and periods. The main imprint of anisotropy can  
468 be seen in the 2D cases (according to WAL isotropic criteria), with strike directions that  
469 are not consistent, or relationships between tensors that would not correspond to  
470 isotropic structures. In these cases, the strike obtained is related to the orientation of the  
471 anisotropy rather than to the structural direction. Table 3 contains the new  
472 dimensionality criteria extended to accommodate these cases with anisotropy and to  
473 distinguish them from isotropic two-dimensionality: anisotropic half-space, a 1D  
474 medium with one anisotropic layer, and an anisotropic 2D medium.

475

476 However, it must be remembered that it is not always possible to identify anisotropy  
477 when the main directions are aligned with the measuring axes, or to retrieve all the

478 parameters that characterize anisotropy from the observed responses and the  
479 dimensionality analysis alone.

480

481 Table 3 considers the dimensionality observed in a particular tensor. In particular  
482 situations described in the text, some patterns can be observed such as that of a 1D  
483 model with two anisotropic layers (2D, 3D and 2D cases, as the period increases).

484

485 Hence, once the dimensionality of the full dataset is obtained (it is recommended to plot  
486 dimensionality maps), one should check for anisotropic imprints and patterns as  
487 described in the text, and evaluate what type of anisotropic media might exist beneath  
488 the survey area.

489

490

## 491 **6. Conclusions**

492 The most important contribution of this study is the demonstration that it is possible to  
493 identify the presence of anisotropy in the dimensionality description given by the WAL  
494 criteria. In addition, we have extended the WAL invariants criteria to differentiate  
495 anisotropic from isotropic media. Hence, when assessing the dimensionality of a dataset  
496 that is considered to contain anisotropy effects, one should follow the original WAL  
497 criteria (Table 1), plus the new conditions described in Table 3. The exception is when  
498 the principal anisotropy directions are aligned with the measuring axes. In this situation,  
499 if the anisotropic media is 2D, the information contained in the induction arrows might  
500 be useful.

501

502 Another important point is that, except in very simple cases, the anisotropy cannot be  
503 identified from one site alone. It is fundamental to check for the consistency of  
504 dimensionality with neighbouring sites or periods.

505

506 Finally, the comparison of the dimensionality description obtained using the WAL  
507 invariant criteria with that from phase tensor diagrams allowed us to conclude that, in  
508 some cases, both provide the same information. However, when the phases do not  
509 change with period, such as in the case of an anisotropic half-space, only the WAL  
510 criteria enable the anisotropy to be identified. It is also important to note that in some  
511 cases the strike angle can only be computed from  $\theta_{3D/2D}$ , which considers the real and  
512 imaginary parts of the tensor, as opposed to the direction defined from the Mohr circles,  
513  $\theta_h$ , which uses the real or the imaginary parts separately.

514

## 515 **6. Acknowledgements**

516 The authors thank Ted Lilley for his critical review, which greatly helped improving the  
517 manuscript. We acknowledge Josef Pek for providing the 2D anisotropic forward code  
518 (Pek and Verner, 1997). This work has been funded by projects CGL2006-10166 and  
519 CGL2009-07604. A. Martí thanks the Universitat de Barcelona and the Department of  
520 Earth Sciences at Memorial University of Newfoundland (MUN) for facilitating her  
521 research term at MUN.

522

523

## 524 **APPENDIX A**

525 In this appendix we first summarize the expressions used to compute the strike  
526 directions from the magnetotelluric tensor using Weaver et al. (2000) notation.

527 Secondly, we derive these expressions for the theoretical magnetotelluric tensors  
 528 corresponding to A) a 2D isotropic structure, rotated an angle  $\theta$  from the strike  
 529 direction, and B) an anisotropic half-space, with the main anisotropic directions rotated  
 530 an angle  $\alpha_S$ .

531

532 1. Strike expressions:

533 The complex parameters  $\zeta_j = \xi_j + i\eta_j$  ( $j = 1, 4$ ), are defined as linear combinations of  
 534 the magnetotelluric tensor components:  $\zeta_1 = (M_{xx} + M_{yy})/2$ ,  $\zeta_2 = (M_{xy} + M_{yx})/2$ ,  
 535  $\zeta_3 = (M_{xx} - M_{yy})/2$  and  $\zeta_4 = (M_{xy} - M_{yx})/2$ :

536

$$537 \quad \underline{M} = \begin{pmatrix} M_{xx} & M_{xy} \\ M_{yx} & M_{yy} \end{pmatrix} = \begin{pmatrix} \zeta_1 + \zeta_3 & \zeta_2 + \zeta_4 \\ \zeta_2 - \zeta_4 & \zeta_1 - \zeta_3 \end{pmatrix} = \begin{pmatrix} \xi_1 + \xi_3 & \xi_2 + \xi_4 \\ \xi_2 - \xi_4 & \xi_1 - \xi_3 \end{pmatrix} + i \begin{pmatrix} \eta_1 + \eta_3 & \eta_2 + \eta_4 \\ \eta_2 - \eta_4 & \eta_1 - \eta_3 \end{pmatrix}. \quad (\text{A1})$$

538

539 If the tensor corresponds to a 2D structure, the strike direction ( $\theta_{2D}$ ) can be computed  
 540 from using either the real or the imaginary parts of  $\zeta_2$  and  $\zeta_3$ , which lead to the same  
 541 result:  $\theta_{2D} = \theta_1 = \theta_2$ :

542

$$543 \quad \tan(2\theta_1) = -\frac{\xi_3}{\xi_2}, \quad (\text{A2})$$

544

545 and

546

$$547 \quad \tan(2\theta_2) = -\frac{\eta_3}{\eta_2}. \quad (\text{A3})$$

548



549 Both the  $\zeta_i$  parameters and the angles  $\theta_1$  and  $\theta_2$  can be represented in Mohr circle  
 550 diagrams (for the real and imaginary parts), which are also used to represent WAL  
 551 invariants (Figure 1).

552

553 If the 2D structure is affected by galvanic distortion, the strike direction ( $\theta_{3D/2D}$ ) can be  
 554 recovered using the expression:

555

$$556 \quad \tan(2\theta_{3D/2D}) = \frac{d_{12} - d_{34}}{d_{13} + d_{24}}, \quad (\text{A4})$$

557

558 where  $d_{ij} = \frac{\xi_i \eta_j - \xi_j \eta_i}{I_1 I_2}$ , and  $I_1$  and  $I_2$  are rotational invariants of the MT tensor.

559

560 Given that 2D is a particular case of 3D/2D (where the galvanic matrix is the identity),  
 561 the same expression works to compute the strike, so that:  $\theta_{2D} = \theta_1 = \theta_2 = \theta_{3D/2D}$ .

562

563 2. Particular cases:

564

565 A. 2D isotropic structure:

$$566 \quad \underline{M}_{2D} = \begin{pmatrix} 0 & M_{xy} \\ M_{yx} & 0 \end{pmatrix}, \quad (\text{A5})$$

567 if the tensor is rotated an angle  $\theta$ :

$$568 \quad \underline{M}' = \underline{R}_\theta \cdot \underline{M}_{2D} \cdot \underline{R}_\theta^T = \begin{pmatrix} (M_{xy} + M_{yx}) \sin \theta \cdot \cos \theta & M_{xy} \cdot \cos^2 \theta - M_{yx} \cdot \sin^2 \theta \\ -M_{xy} \cdot \sin^2 \theta + M_{yx} \cdot \cos^2 \theta & -(M_{xy} + M_{yx}) \cdot \sin \theta \cdot \cos \theta \end{pmatrix}, \quad (\text{A6})$$

569

570 and:

$$\zeta_1 = 0$$

$$571 \quad \zeta_2 = (M_{xy} + M_{yx}) \cdot (\sin^2 \theta - \cos^2 \theta) / 2 \quad (A7)$$

$$\zeta_3 = (M_{xy} + M_{yx}) \cdot \sin \theta \cdot \cos \theta,$$

$$\zeta_4 = (M_{xy} - M_{yx}) / 2$$

$$572 \quad \tan(2\theta_1) = -\frac{\operatorname{Re}(M_{xy} + M_{yx}) \cdot \sin \theta \cdot \cos \theta}{\operatorname{Re}(M_{xy} + M_{yx}) \left( \frac{\sin^2 \theta - \cos^2 \theta}{2} \right)} = -\frac{2 \cdot \sin \theta \cdot \cos \theta}{\sin^2 \theta - \cos^2 \theta} = -\frac{\sin(2\theta)}{-\cos(2\theta)} = \tan(2\theta), \quad (A8)$$

573 and

$$574 \quad \tan(2\theta_2) = -\frac{\operatorname{Im}(M_{xy} + M_{yx}) \cdot \sin \theta \cdot \cos \theta}{\operatorname{Im}(M_{xy} + M_{yx}) \left( \frac{\sin^2 \theta - \cos^2 \theta}{2} \right)} = -\frac{2 \cdot \sin \theta \cdot \cos \theta}{\sin^2 \theta - \cos^2 \theta} = -\frac{\sin(2\theta)}{-\cos(2\theta)} = \tan(2\theta). \quad (A9)$$

575 This proves that  $\theta_{2D} = \theta_1 = \theta_2 = \theta$ .

576

577 Using the expression in A4:.

$$578 \quad d_{12} = d_{13} = 0,$$

$$579 \quad d_{34} = \frac{\operatorname{Re}(M_{xy} + M_{yx}) \cdot \sin \theta \cdot \cos \theta \cdot \frac{\operatorname{Im}(M_{xy} - M_{yx})}{2} - \frac{\operatorname{Re}(M_{xy} - M_{yx})}{2} \cdot \operatorname{Im}(M_{xy} + M_{yx}) \cdot \sin \theta \cdot \cos \theta}{I_1 \cdot I_2},$$

$$580 \quad d_{24} = \frac{\operatorname{Re}(M_{xy} + M_{yx}) \cdot \frac{(\sin^2 \theta - \cos^2 \theta)}{2} \cdot \frac{\operatorname{Im}(M_{xy} - M_{yx})}{2} - \frac{\operatorname{Re}(M_{xy} - M_{yx})}{2} \cdot \operatorname{Im}(M_{xy} + M_{yx}) \cdot \frac{(\sin^2 \theta - \cos^2 \theta)}{2}}{I_1 \cdot I_2}.$$

581

Hence:

$$582 \quad \tan(2\theta_{3D/2D}) = \frac{-d_{34}}{d_{24}} = -2 \cdot \frac{(\operatorname{Im}(M_{xy} + M_{yx}) \cdot \operatorname{Re}(M_{xy} - M_{yx}) - \operatorname{Re}(M_{xy} + M_{yx}) \cdot \operatorname{Im}(M_{xy} - M_{yx})) \cdot \sin \theta \cdot \cos \theta}{(\operatorname{Im}(M_{xy} + M_{yx}) \cdot \operatorname{Re}(M_{xy} - M_{yx}) - \operatorname{Re}(M_{xy} + M_{yx}) \cdot \operatorname{Im}(M_{xy} - M_{yx})) \cdot (\sin^2 \theta - \cos^2 \theta)}$$

583

$$584 \quad = \frac{-2 \cdot \sin \theta \cos \theta}{\sin^2 \theta - \cos^2 \theta} = \frac{-\sin(2\theta)}{-\cos(2\theta)} = \tan(2\theta),$$

585

which proves that:

$$586 \quad \theta_{3D/2D} = \theta_1 = \theta_2 = \theta.$$

587

588 B. Anisotropic half-space:

589

590 The analytic expression of the MT tensor corresponding to an anisotropic half-space,  
591 with the main anisotropic directions rotated an angle  $\alpha_s$  is obtained using the  
592 development from Pek and Santos (2002):

593

$$594 \quad \underline{M}_{anis} = C \cdot \begin{pmatrix} d \cdot \sin(2\alpha_s) & -s - d \cdot \cos(2\alpha_s) \\ s - d \cdot \cos(2\alpha_s) & -d \cdot \sin(2\alpha_s) \end{pmatrix} (i+1),$$

595 where C is a constant,  $s = \sqrt{\rho'_{xx}} + \sqrt{\rho'_{yy}}$  and  $d = \sqrt{\rho'_{xx}} - \sqrt{\rho'_{yy}}$ .

$$\zeta_1 = 0$$

$$\zeta_2 = -C \cdot \frac{d}{2} \cos(2\alpha_s)(1+i)$$

596

$$\zeta_3 = C \cdot \frac{d}{2} \sin(2\alpha_s)(1+i)$$

$$\zeta_4 = C \cdot s \cdot (1+i)$$

597 Given that both the real and imaginary parts have the same value,

$$598 \quad \tan(2\theta_1) = \tan(2\theta_2) = -\frac{\frac{d}{2} \sin(2\alpha_s)}{-\frac{d}{2} \cos(2\alpha_s)} = \tan(2\alpha_s),$$

599 which proves that  $\theta_{2D} = \theta_1 = \theta_2 = \alpha_s$ .

600

601 On the other hand, if the strike direction is computed using the expression of  $\theta_{3D/2D}$ ,  $d_{ij} =$   
602 0, for any  $i, j$  because real and imaginary parts of the tensor are identical. Consequently:

$$603 \quad \tan(2\theta_{3D/2D}) = \frac{0}{0}, \text{ which is an undetermination.}$$

604

605 **References**

- 606 Caldwell, T.G., Bibby, H.M., Brown, C., 2004. The Magnetotelluric Phase Tensor.  
607 *Geophys. J. Int.*, 158, 457-469.
- 608 Cantwell, T., 1960. Detection and analysis of low frequency magnetotelluric signals.  
609 Ph.D. Thesis, Dept. of Geology and Geophysics, M.I.T. Cambridge, MA.
- 610 Eaton, D.W., Jones, A.G., 2006. Tectonic fabric of the subcontinental lithosphere:  
611 Evidence from seismic, magnetotelluric and mechanical anisotropy. *Phys. Earth  
612 Planet. Inter.*, 158, 85-91.
- 613 Fischer, G., Masero, W., 1994. Rotational properties of the magnetotelluric impedance  
614 tensor, the example of the Araguinha impact crater, Brazil. *Geophys. J. Int.*,  
615 119, 548-560.
- 616 Gatzemeier, A., Tommasi, A., 2006. Flow and electrical anisotropy in the upper mantle:  
617 Finite-element models constraints on the effects of olivine crystal preferred  
618 orientation and microstructure. *Phys. Earth Planet. Inter.*, 158, 92-106.
- 619 Groom, R.W., Bailey, R.C., 1989. Decomposition of the magnetotelluric impedance  
620 tensor in the presence of local three-dimensional galvanic distortion. *J. Geophys.  
621 Res.*, 94, 1913-1925.
- 622 Heise, W., Pous, J., 2003. Anomalous phases exceeding 90° in magnetotellurics:  
623 anisotropic model studies and a field example. *Geophys. J. Int.*, 155, 308-318.
- 624 Heise, W., Caldwell, T.G., Bibby, H.M., Brown, C., 2006. Anisotropy and phase splits  
625 in magnetotellurics. *Phys. Earth Planet. Inter.*, 158, 107-121.
- 626 Jones, A.G., 1993. The COPROD2 dataset: Tectonic setting, recorded MT data and  
627 comparison of models. *J. Geomagn. Geoelectr.*, 45, 933-955.
- 628 Jones, A.G., 2006. Electromagnetic interrogation of the anisotropic Earth: Looking into  
629 the Earth with polarized spectacles. *Phys. Earth Planet. Inter.*, 158, 281-291.

- 630 Jones, A.G., Craven, J.A., 1990. The North American Central Plains conductivity  
631 anomaly and its correlation with gravity, magnetics, seismic, and heat flow data  
632 in the Province of Saskatchewan. *Phys. Earth Planet. Inter.*, 60, 169-194.
- 633 Jones, A.G., Craven, J.A., McNeice, G.A., Ferguson, I.J., Boyce, T., Farquharson, C.,  
634 Ellis, R.G., 1993. The North American Central Plains conductivity anomaly  
635 within the Trans-Hudson orogen in northern Saskatchewan. *Geology*, 21, 1027-  
636 1030.
- 637 Kaufman, A. A., 1988. Reduction of the geological noise in magnetotelluric soundings.  
638 *Geoexploration*, 25, 145-161.
- 639 Li, Y., 2002. A finite-element algorithm for electromagnetic induction in two-  
640 dimensional anisotropic conductivity structures. *Geophys. J. Int.*, 148, 389-401.
- 641 Lilley, F.E.M., 1993. Magnetotelluric analysis using Mohr circles. *Geophysics*, 58,  
642 1498-1506.
- 643 Lilley, F.E.M., 1998a. Magnetotelluric tensor decomposition: Part I, Theory for a basic  
644 procedure. *Geophysics*, 63, 1885-1897.
- 645 Lilley, F.E.M., 1998b. Magnetotelluric tensor decomposition: Part II, Examples of a  
646 basic procedure. *Geophysics*, 63, 1898-1907.
- 647 Lilley, F.E.M., Weaver, J.T., 2009. Phases greater than 90° in MT data: Analysis using  
648 dimensionality tools. *Journal of Applied Geophysics*, 70, 9-16.
- 649 Martí, A., Queralt, P., Roca, E., 2004. Geoelectric dimensionality in complex geologic  
650 areas: application to the Spanish Betic Chain. *Geophys. J. Int.*, 157, 961-974.
- 651 Martí, A., Queralt, P., Ledo, J., 2009. WALDIM: A code for the dimensionality analysis  
652 of magnetotelluric data using the rotational invariants of the magnetotelluric  
653 tensor. *Comp. Geosci.*, 35, 2295-2303.

- 654 McNeice, G., Jones, A.G., 2001. Multisite, multifrequency tensor decomposition of  
655 magnetotelluric data. *Geophysics*, 66, 158-173.
- 656 Negi, J.G. and Saraf, P.D., 1989, Anisotropy in Geoelectromagnetism,. *Methods in*  
657 *geochemistry and geophysics*, 28, Elsevier (Amsterdam).
- 658 Osella, A.M., Martinelli, P., 1993. Magnetotelluric response of anisotropic 2-D  
659 structures. *Geophys. J. Int.*, 115, 819-828.
- 660 Pek, J., Santos, F.A.M., 2002. Magnetotelluric impedances and parametric sensitivities  
661 for 1-D anisotropic media, *Comp. Geosci.*, 28, 939-950.
- 662 Pek, J., Santos, F.A.M., 2006. Magnetotelluric inversion for anisotropic conductivities  
663 in layered media. *Phys. Earth Planet. Inter.*, 158, 139-158.
- 664 Pek, J., Verner, T., 1997. Finite-difference modelling of magnetotelluric fields in two-  
665 dimensional anisotropic media. *Geophys. J. Int.*, 128, 505–521.
- 666 Reddy, I.K., Rankin, D., 1975. Magnetotelluric response of laterally inhomogeneous  
667 and anisotropic media. *Geophysics*, 40, 1035-1045.
- 668 Saraf, P.D., Negi, J.G., Cerv, V., 1986. Magnetotelluric response of a laterally  
669 inhomogeneous anisotropic inclusion. *Phys. Earth Planet. Inter.*, 43, 196-198.
- 670 Simpson, F., Bahr, K., 2005. *Practical Magnetotellurics*. Cambridge University Press.
- 671 Smith, J.T., 1995. Understanding telluric distortion matrices. *Geophys. J. Int.*, 122, 219-  
672 226.
- 673 Szarka, L., Menvielle, M., 1997. Analysis of rotational invariants of the magnetotelluric  
674 impedance tensor. *Geophys. J. Int.*, 129, 133-142.
- 675 Vozoff, K., 1991. The magnetotelluric method. In: *Electromagnetic Methods in Applied*  
676 *Geophysics – Vol 2. Applications*. Soc. Expl. Geophys., Tulsa, OK.
- 677 Wang, T., Fang, S., 2001. 3-D electromagnetic anisotropy modeling using finite  
678 differences. *Geophysics*, 66, 1386-1398.

- 679 Wang, D., Mookherjee, M., Xu, Y., Karato, S., 2006. The effect of water on the  
680 electrical conductivity of olivine. *Nature*, 443, 977-980.
- 681 Wannamaker, P.E., 2005. Anisotropy versus heterogeneity in continental solid Earth  
682 electromagnetic studies: Fundamental response characteristics and implications  
683 for physicochemical state. *Surv. Geophys.*, 26, 733-765.
- 684 Weaver, J.T., Agarwal, A.K., Lilley, F.E.M., 2000. Characterisation of the  
685 magnetotelluric tensor in terms of its invariants. *Geophys. J. Int.*, 141, 321-336.
- 686 Weidelt, P., 1999. 3D conductivity models: implications of electrical anisotropy. In:  
687 Oristaglio, M., Spies, B. (eds.): *Three-Dimensional Electromagnetics*. Society of  
688 Exploration Geophysicists, Tulsa (OK), 119-137.
- 689 Yin, C., 2003. Inherent nonuniqueness in magnetotelluric inversion for 1D anisotropic  
690 models. *Geophysics*, 68, 138-146.
- 691 Yoshino, T., Matsuzaki, T., Yamashita, S., Katsura, T., 2006. Hydrous olivine unable to  
692 account for conductivity anomaly at the top of the asthenosphere. *Nature*, 443,  
693 973-976.
- 694

695 **Figure captions:**

696 Figure 1: Diagram of the real and imaginary Mohr circles generated after a complete  
 697 rotation of the  $M_{xy}$  and  $M_{xx}$  components of the MT tensor. In black: parameters and  
 698 circle associated with the real part. Grey: the equivalent for the imaginary part. After  
 699 Lilley (1998a).

700

701 Figure 2: Diagram of successive Euler rotations applied to generate any orientation of  
 702 the anisotropic principal directions, using the anisotropy strike ( $\alpha_S$ ), dip ( $\alpha_D$ ) and slant  
 703 ( $\alpha_L$ ) angles.

704

705 Figure 3: a) Dimensionality and apparent resistivity responses for the three anisotropic  
 706 half-space models (**1a**, **1b** and **1c**), at one single site (located at the centre of the model)  
 707 for the computed periods. Strike directions are shown assuming a 2D structure ( $\theta_{2D}$ ) and  
 708 assuming galvanic distortion over a 2D model ( $\theta_{3D/2D}$ ) (except at model **1a** where the  
 709 two directions are coincident). xx and yy apparent resistivities in model **1a** are null and  
 710 hence not shown. b) Left: Mohr diagram for the responses of model **1c**. Both real and  
 711 imaginary circles are coincident and agree with a 2D structure. Right: Mohr diagram for  
 712 a single period,  $T = 1$  s, of model **1c** showing the main parameters, and the strike angles  
 713  $\theta_1$  and  $\theta_2$  (coincident with  $\theta_h$ , eqs. 113 and 114 in Lilley, 1998a). Note that  $\theta_{3D/2D}$   
 714 cannot be represented using Mohr circles.

715

716 Figure 4: Cross section of model 2a, corresponding to a layered model with an  
 717 anisotropic layer, and resistivity and phase responses obtained at any site of the model.  
 718 The off-diagonal resistivity and phases are plotted together with the responses of a



719 model with an isotropic layer of 100  $\Omega\cdot\text{m}$  and a model with an anisotropic layer of 1  
720  $\Omega\cdot\text{m}$ .

721

722 Figure 5: Top: Cross sections of models **2b** and **2c**, consisting of 1D models with two  
723 anisotropic layers. Bottom: Dimensionality pattern of the corresponding responses, with  
724 the principal angles and distortion angles indicated.

725

726 Figure 6: Cross-section of models **3a**, **3b** and **3c** and the corresponding dimensionality  
727 patterns. Only one out of every 4 sites are plotted. For model **3a**, in the 2D cases, the  
728 strike angle is  $0^\circ$ .

729

730 Figure 7: Cross-sections of models **4a** and **4b** (from Heise et al., 2006), used to compute  
731 the responses from general 2D models with anisotropic structures.

732

733 Figure 8: Dimensionality patterns corresponding to the responses of models **4a** and **4b**  
734 and **4c**. All sites where responses have been computed are shown. Blank zones inside  
735 the diagrams correspond to cases for which none of the defined criteria were met and  
736 hence for which the dimensionality could not be determined.

737

738 Figure 9: Phase tensor diagrams corresponding to site 1 (located at km 0) for models **4a**  
739 and **4b**. The horizontal axis indicates the value of the phase tangent. These diagrams are  
740 very similar to those obtained for the last site (site 33, located at km 250).

741

742 Figure 10: Phase tensor diagrams corresponding to the responses of model **4c**, for 5  
743 periods between 1 s and 10000 s. One out of every two sites is shown, except between

744 100 km and 150 km, where only one out of every 4 sites is represented. The minor and  
745 major axes of the ellipses indicate the value of the phase tangent in the way that the  
746 radii of the circles at 1 s are equal to 1.

747

748 Figure 11: Dimensionality cases for: a) the responses of the anisotropic model presented  
749 by Jones (2006), which fits the off-diagonal components of site 85\_314 in the  
750 COPROD2 dataset; and b) for all the components of site 85\_314 from the COPROD2  
751 dataset (modified from Martí et al., 2009).

752

753

754

755 **Table captions:**

756 Table 1: Dimensionality criteria according to the WAL invariant values of the  
757 magnetotelluric tensor (modified from Weaver et al., 2000). Row “2D” with the grey  
758 background is extended in Table 3, where structures with anisotropy are considered.

759

760 Table 2: Resistivity values and orientations of the three anisotropic half-space models

761 **1a, 1b and 1c.**

762

763 Table 3: Dimensionality criteria extended to anisotropic structures, characterized by the  
764 WAL invariants criteria indicating isotropic 2D.

765

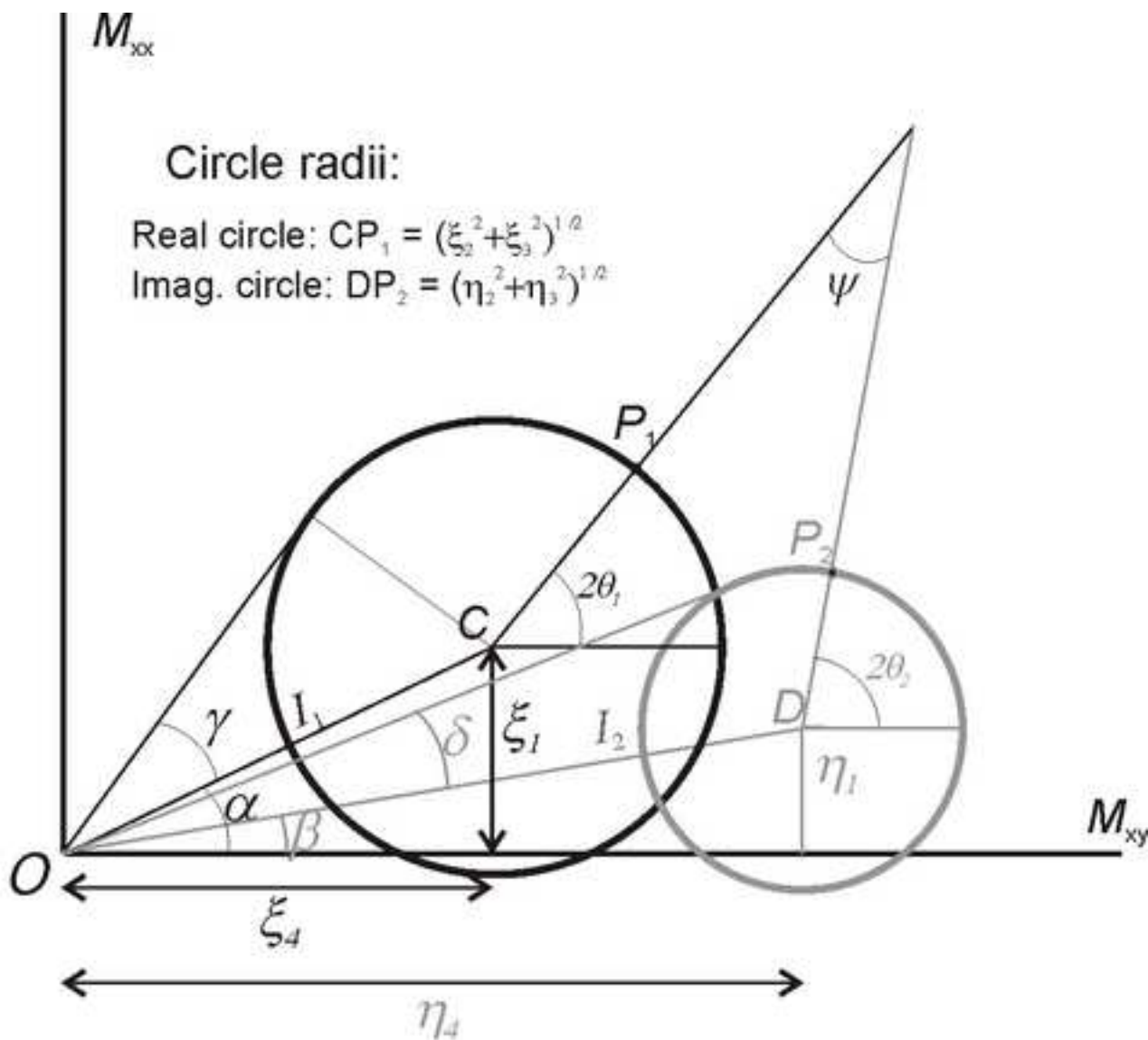


Figure 1. Martí et al.

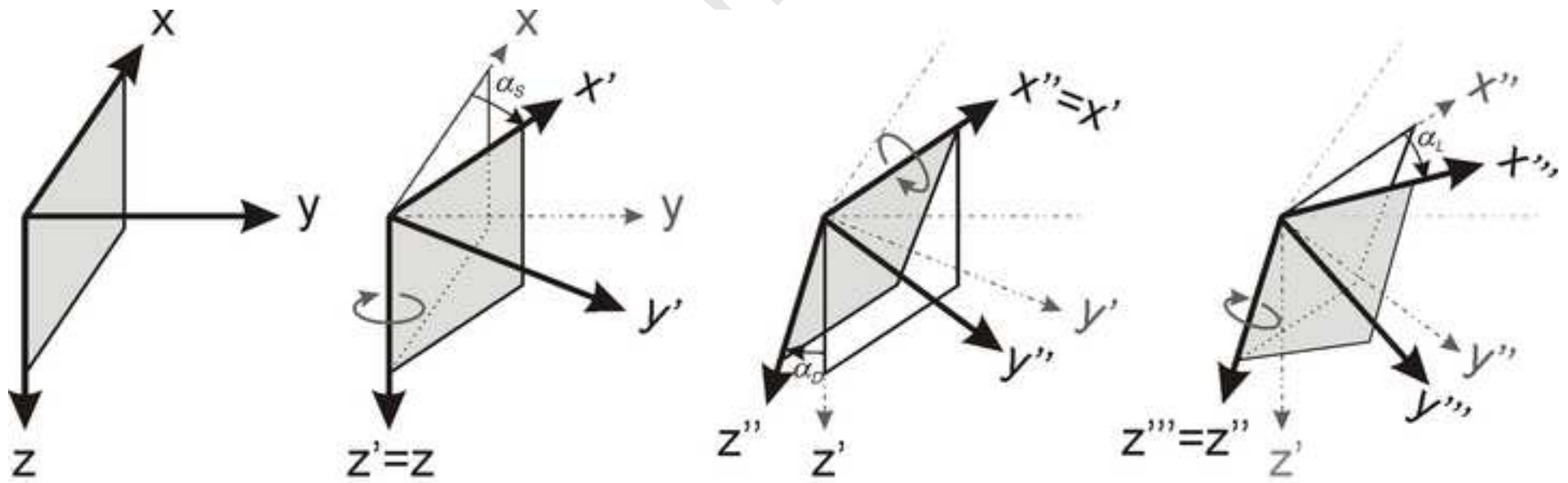


Figure 2. Martí et al.

Figure 3  
[Click here to download high resolution image](#)

Azimuthal anisotropy 50 / 500 / 500  $\Omega\cdot\text{m}$

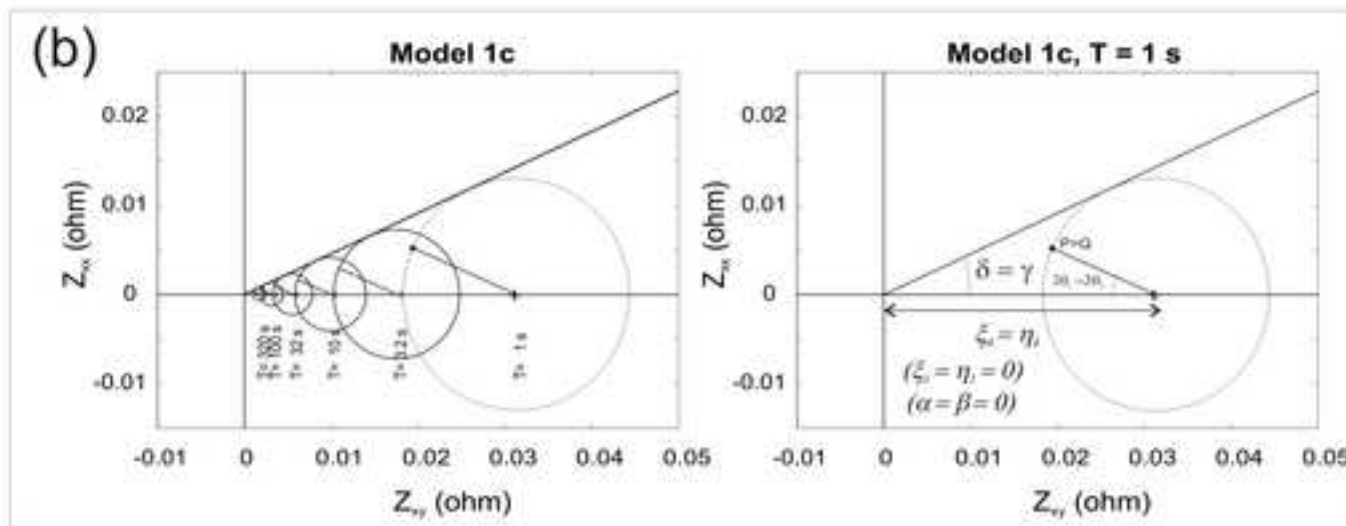
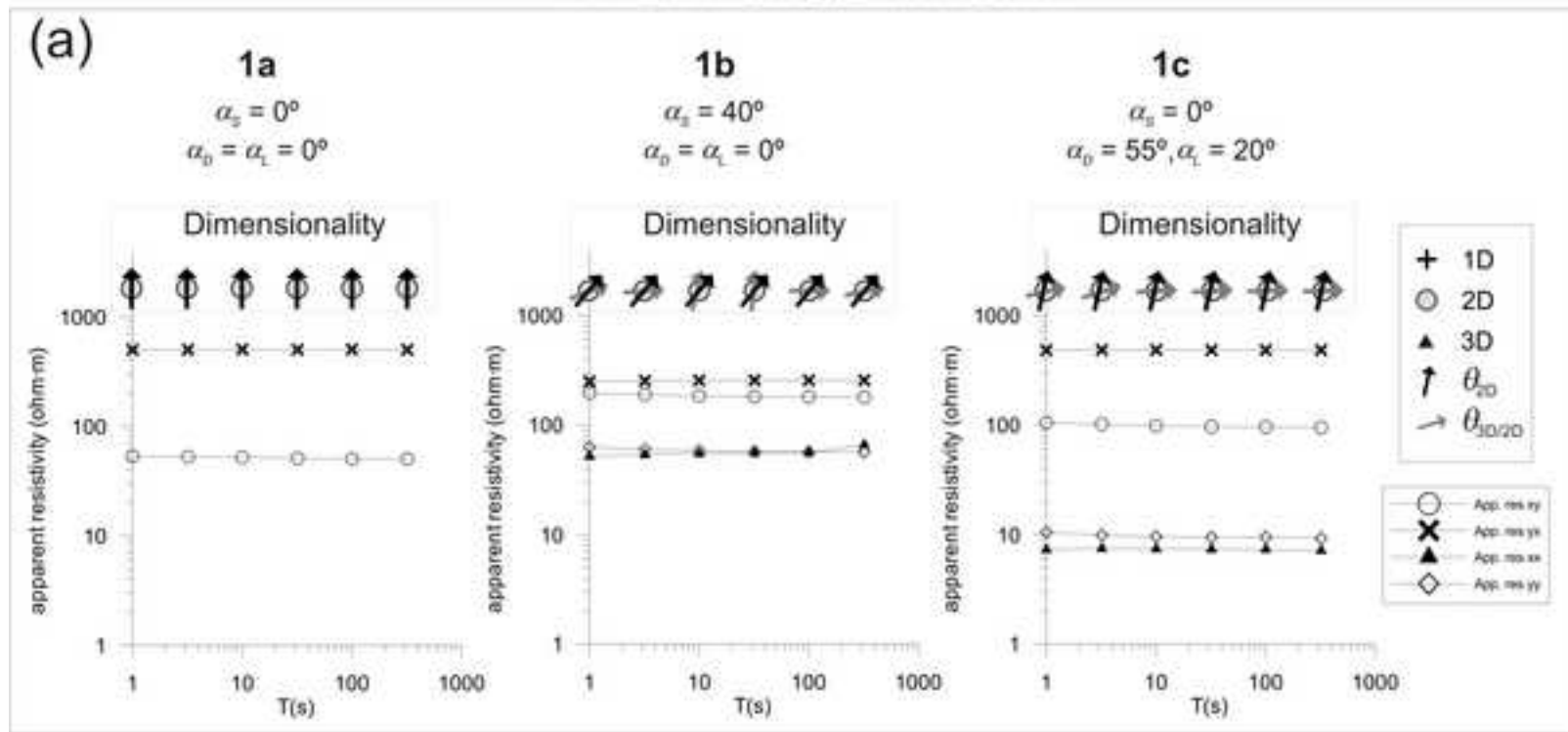


Figure 3. Martí et al.

Figure 4  
[Click here to download high resolution image](#)

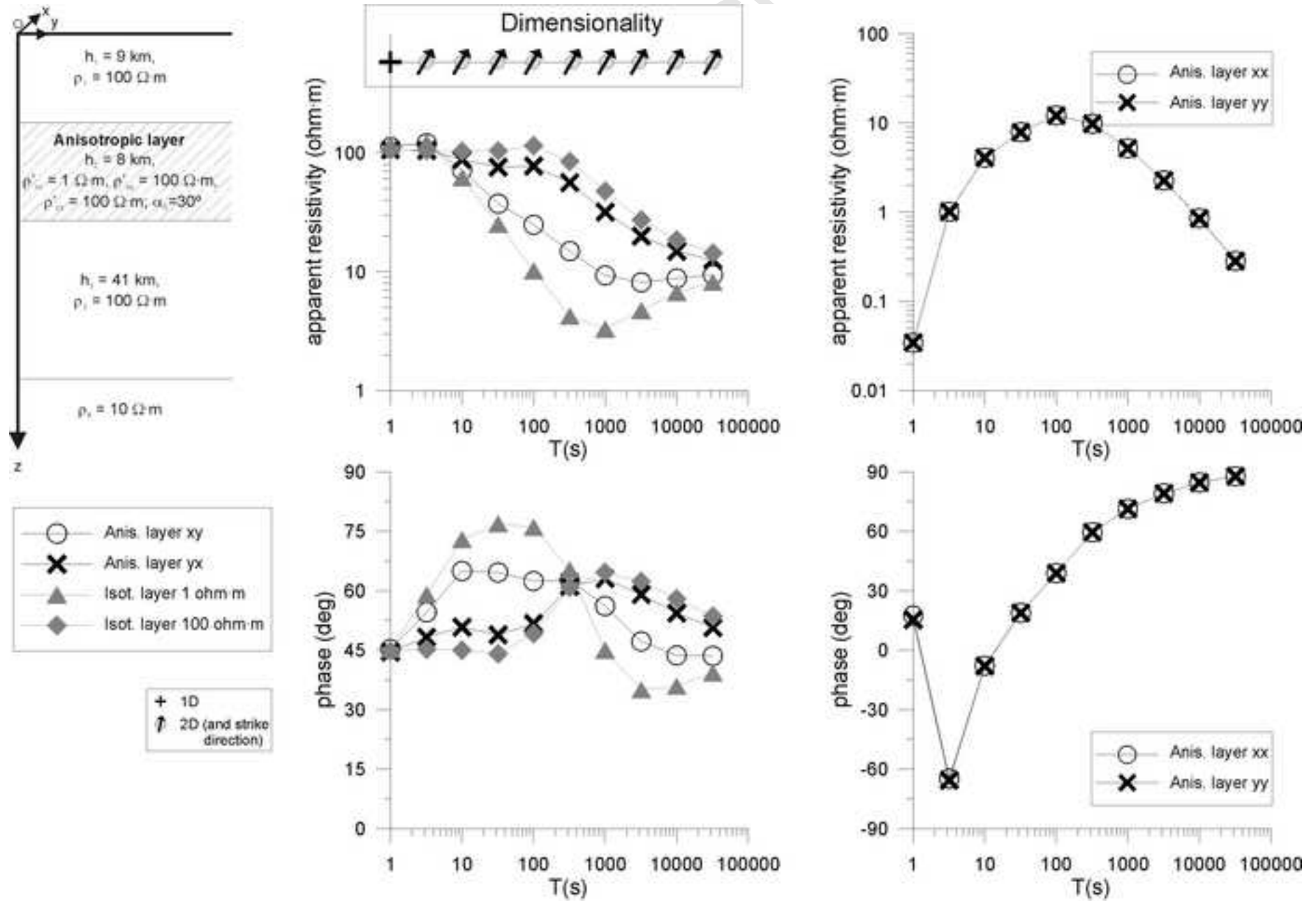


Figure 4. Marti et al.

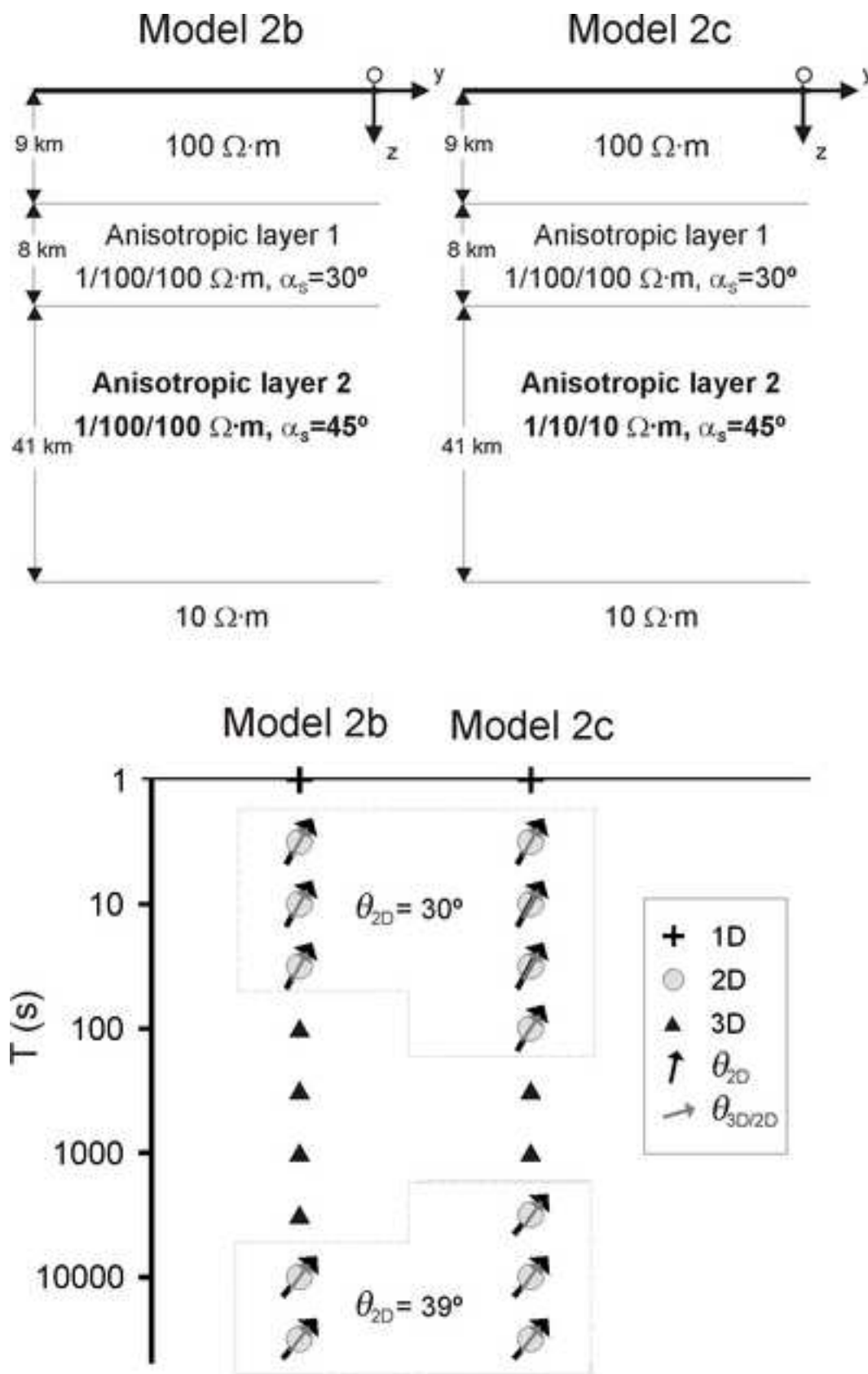


Figure 5. Martí et al.

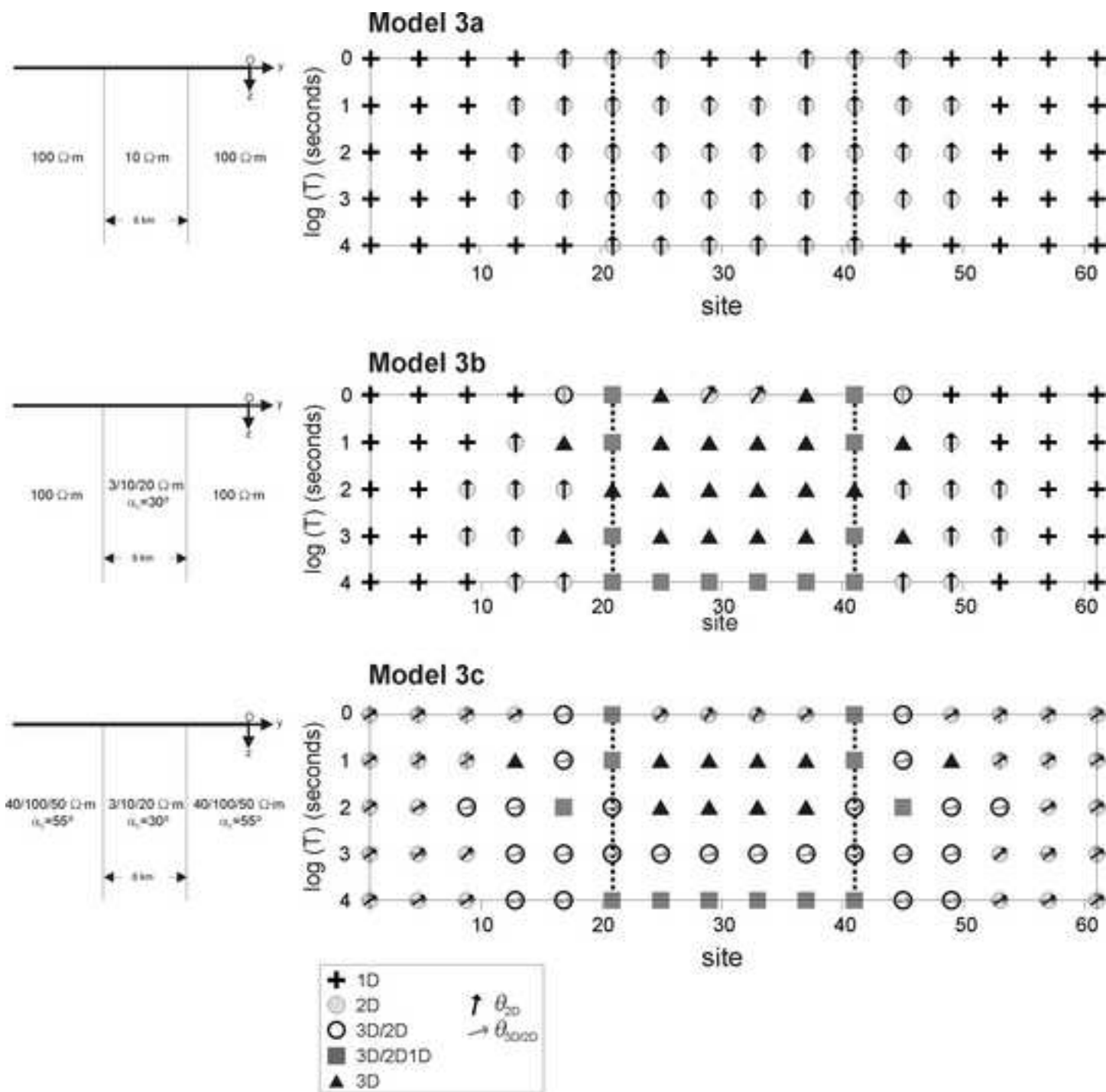


Figure 6. Martí et al.



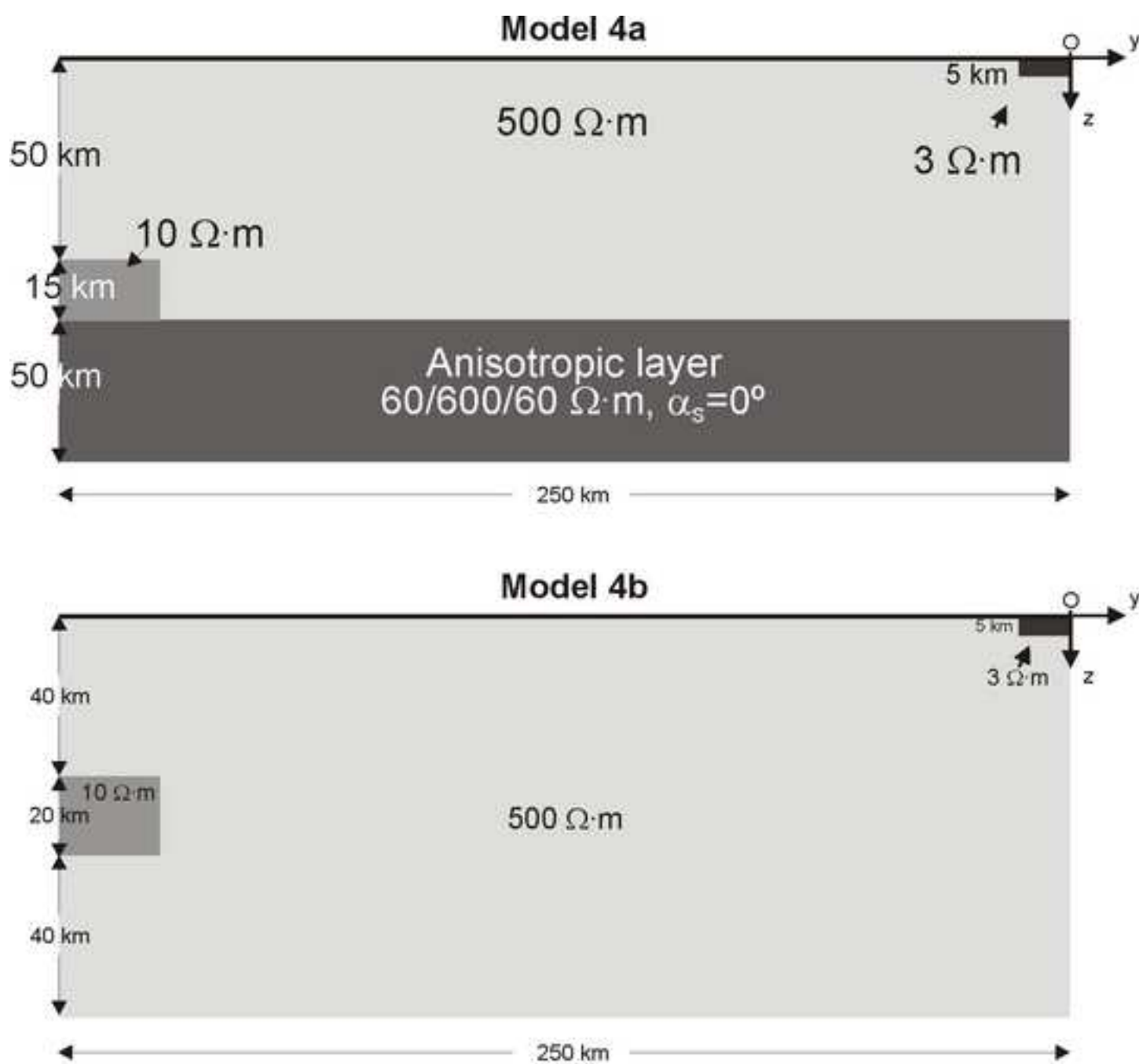


Figure 7. Martí et al.

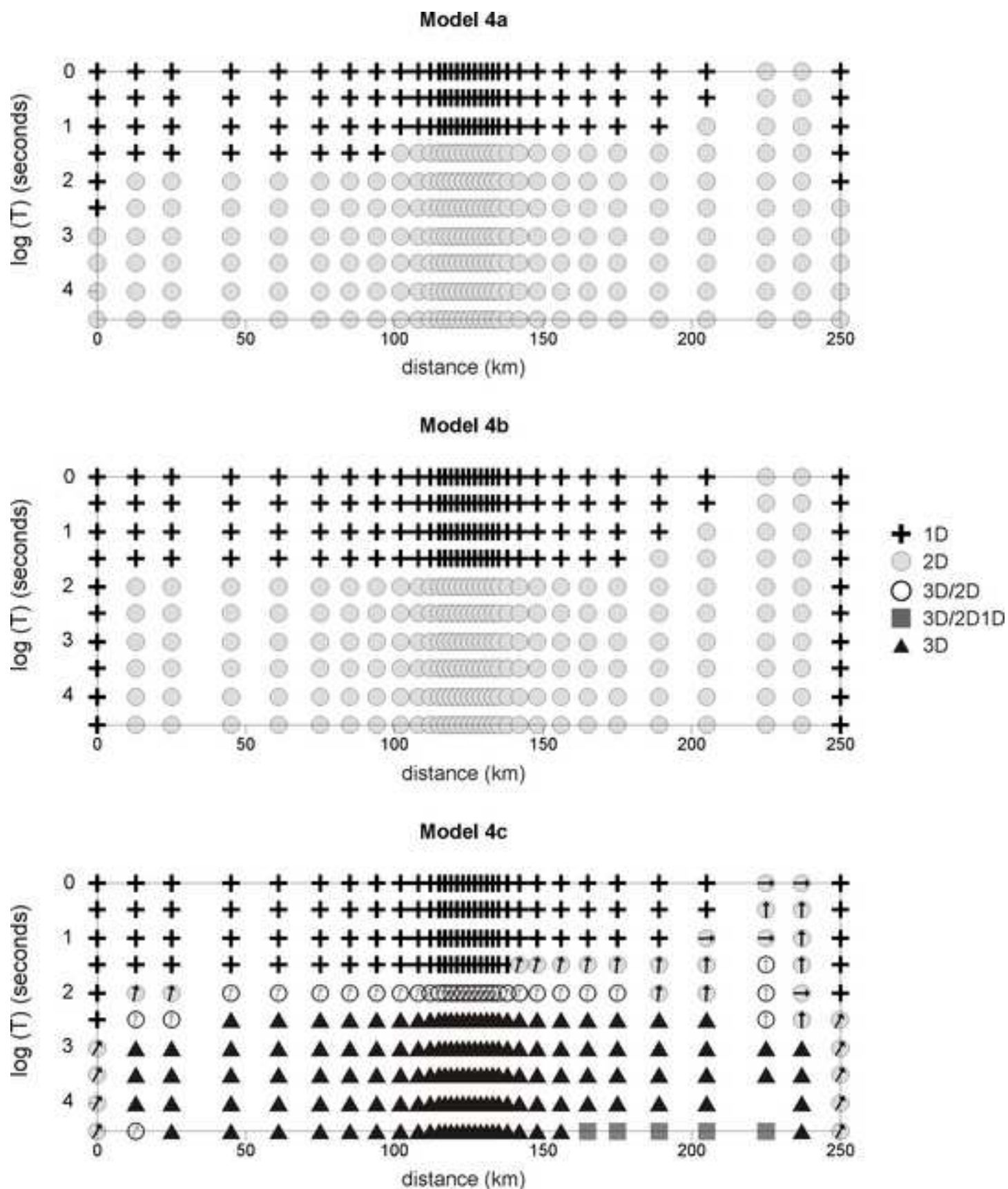


Figure 8. Martí et al.

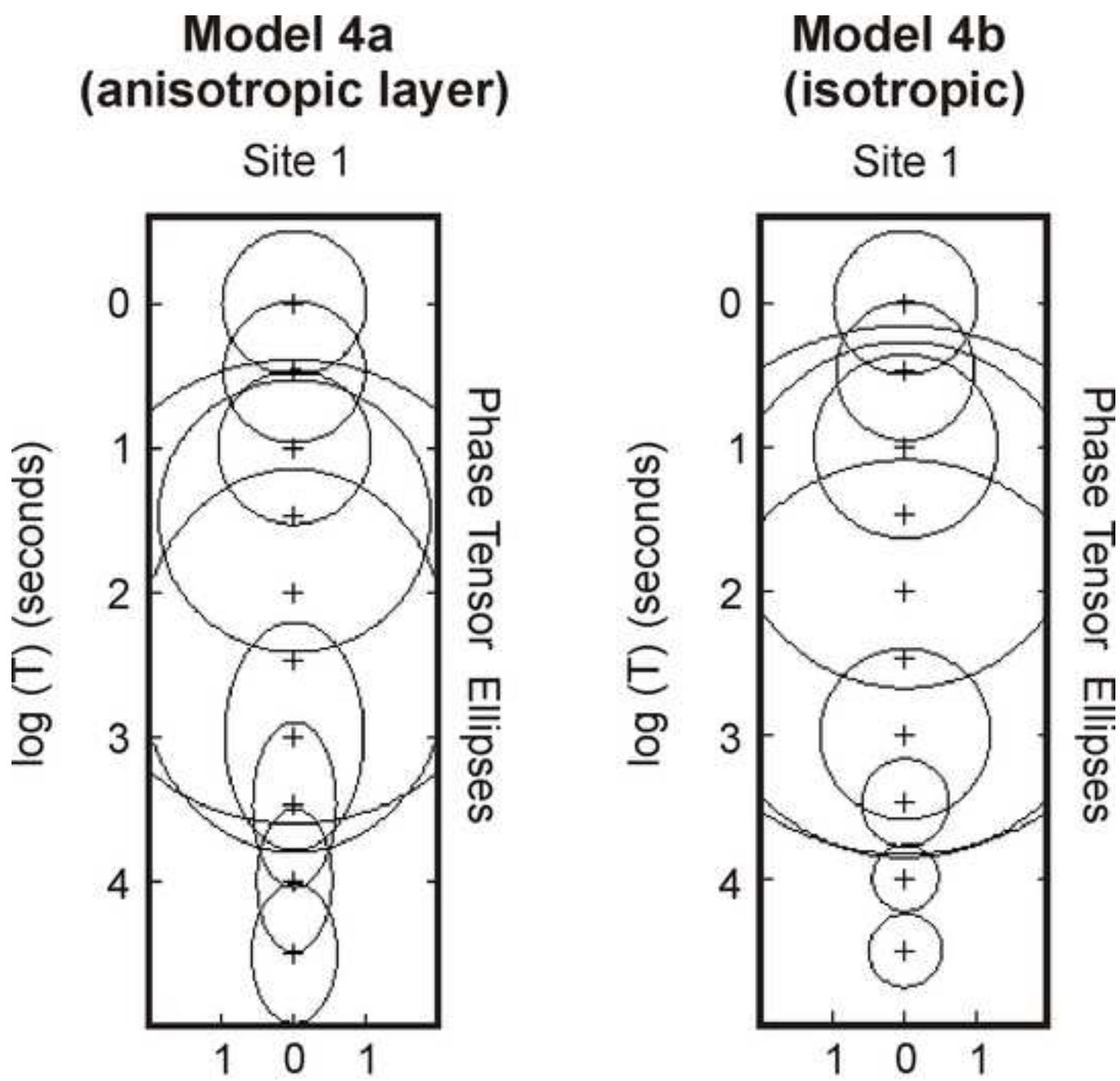


Figure 9. Martí et al.

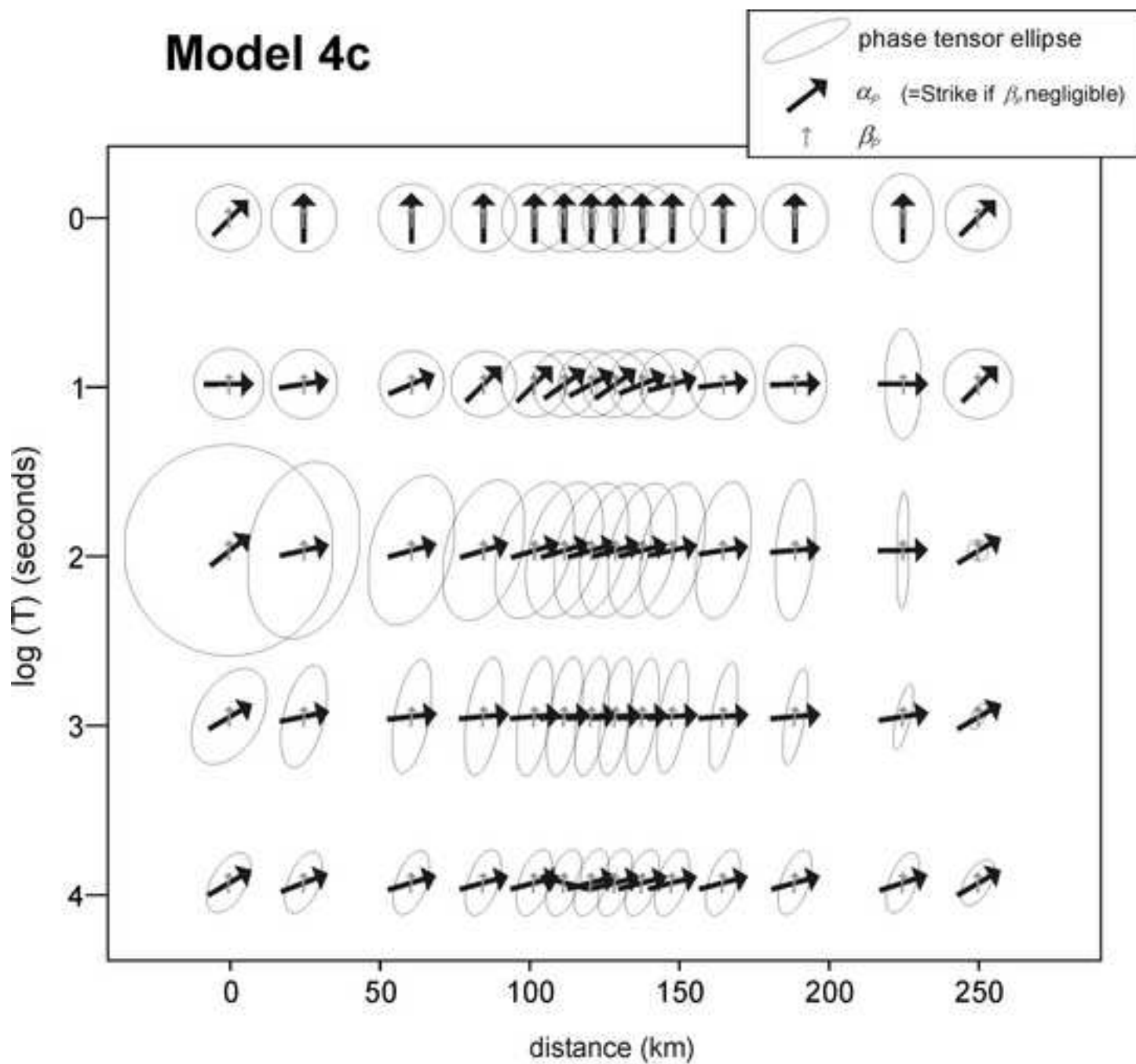


Figure 10. Martí et al.

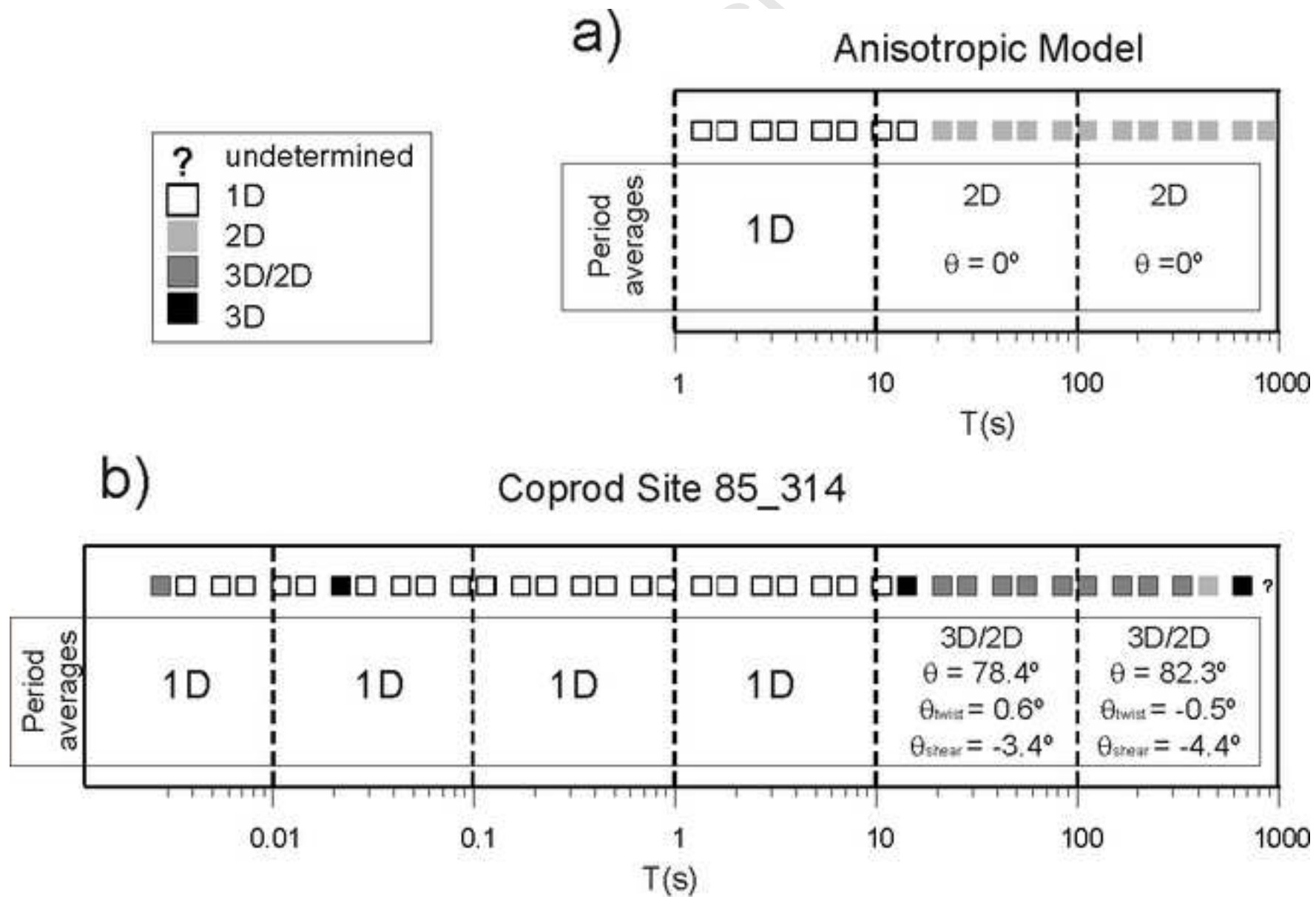


Figure 11. Martí et al.

Case	$I_3$ to $I_7$ and Q values	GEOELECTRIC DIMENSIONALITY
1	$I_3 = I_4 = I_5 = I_6 = 0$	<b>1D</b> $\rho_{1D} = \mu_0 \frac{(I_1^2 + I_2^2)}{\omega}$ , $\varphi_{1D} = \arctan\left(\frac{I_2}{I_1}\right)$
2	$I_3 \neq 0$ or $I_4 \neq 0$ ; $I_5 = I_6 = 0$ ; $I_7 = 0$ or $Q = 0$ ( $\xi_4 \neq 0$ and $\eta_4 \neq 0$ )	<b>2D</b>
3a	$I_3 \neq 0$ or $I_4 \neq 0$ ; $I_5 \neq 0$ ; $I_6 = 0$ ; $I_7 = 0$	<b>3D/2Dtwist</b> 2D affected by galvanic distortion (only twist)
3b	$I_3 \neq 0$ or $I_4 \neq 0$ ; $I_5 \neq 0$ ; $I_6 = 0$ ; $Q = 0$	<b>3D/1D2D</b> Galvanic distortion over a 1D or 2D structure (non-recoverable strike direction)
3c	$I_3 \neq 0$ or $I_4 \neq 0$ ; $I_5 = I_6 = 0$ ; $I_7 = 0$ or $Q = 0$ ( $\xi_4 = 0$ and $\eta_4 = 0$ )	<b>3D/1D2Ddiag</b> Galvanic distortion over a 1D or 2D structure resulting in a diagonal MT tensor
4	$I_3 \neq 0$ or $I_4 \neq 0$ ; $I_5 \neq 0$ ; $I_6 \neq 0$ ; $I_7 = 0$	<b>3D/2D</b> General case of galvanic distortion over a 2D structure
5	$I_7 \neq 0$	<b>3D</b> (affected or not by galvanic distortion)

Table 1. Martí *et al.*

<b>Homogeneous models</b> $\rho'_{xx} = 50 \text{ } \Omega \cdot \text{m}$ and $\rho'_{yy} = \rho'_{zz} = 500 \text{ } \Omega \cdot \text{m}$	<b>Anisotropy angles</b>
Model <b>1a</b>	$\alpha_S = 0^\circ, \alpha_D = 0^\circ, \alpha_L = 0^\circ$
Model <b>1b</b>	$\alpha_S = 40^\circ, \alpha_D = 0^\circ, \alpha_L = 0^\circ$
Model <b>1c</b>	$\alpha_S = 0^\circ, \alpha_D = 55^\circ, \alpha_L = 20^\circ$

Table 2. Martí et al.

Accepted Manuscript

$I_3$ to $I_7$ and Q	GEOELECTRIC DIMENSIONALITY ("2D cases")			
$I_3 \neq 0$ or $I_4 \neq 0$ ; $I_5 = I_6 = 0$ ; $I_7 = 0$ or Q = 0	$\theta_{2D} = \theta_1 = \theta_2 = \theta_{3D/2D}$	Identical tensors at all sites (period dependent)	$\theta_{2D} = 0$	<b>1D MEDIUM WITH ONE ANISOTROPIC LAYER or 2D ISOTROPIC MEDIUM WITH MEASUREMENTS ALONG STRIKE</b>
			$\theta_{2D} \neq 0$	<b>1D MEDIUM WITH ONE ANISOTROPIC LAYER</b>
		Different tensors at each site (period dependent)		<b>2D ISOTROPIC MEDIUM</b>
	$\theta_{2D} \neq \theta_{3D/2D}$	Identical tensors at all sites (period independent)		<b>HOMOGENEOUS ANISOTROPIC MEDIUM</b>
	$\theta_{2D} \neq \theta_{3D/2D}$ or $\theta_1 \neq \theta_2$	Different tensors at each site (period dependent)		<b>ANISOTROPIC STRUCTURE IN A 2D MEDIUM</b>

Table 3. Martí et al.